Determination of $\sin^2\vartheta^{eff}\_W$ using jet charge measurements in hadronic Z decays

D. Buskulic, I. de Bonis, D. Decamp, P. Ghez, C. Goy, J.P. Lees, A. Lucotte, M.N. Minard, P. Odier, B. Pietrzyk, et al.

Z. Phys. C 71, 357–378 (1996)

ZEITSCHRIFT
FÜR PHYSIK C

Determination of $\sin^2 \theta_w^{eff}$ using jet charge measurements in hadronic Z decays

ALEPH Collaboration

D. Buskulic, I. De Bonis, D. Decamp, P. Ghez, C. Goy, J.-P. Lees, A. Lucotte, M.-N. Minard, P. Odier, B. Pietrzyk
Laboratoire de Physique des Particules (LAPP), IN^2P^3-CNRS, 74019 Annecy-le-Vieux Cedex, France

M. Chmeissani, J.M. Crespo, M. Delfino,[12] I. Efthymiopoulos, E. Fernandez, M. Fernandez-Bosman, Ll. Garrido,[15] A. Juste, M. Martinez, S. Orteu, A. Pacheco, C. Padilla, A. Pascual, J.A. Perlas, I. Riu, F. Sanchez, F. Teubert
Institut de Fisica d'Altes Energies, Universitat Autonoma de Barcelona, 08193 Bellaterra (Barcelona), Spain[7]

A. Colaleo, D. Creanza, M. de Palma, G. Gelao, M. Girone, G. Iaselli, G. Maggi,[3] M. Maggi, N. Marinelli, S. Nuzzo, A. Ranieri, G. Raso, F. Ruggieri, G. Selvaggi, L. Silvestris, P. Tempesta, G. Zito
Dipartimento di Fisica, INFN Sezione di Bari, 70126 Bari, Italy

X. Huang, J. Lin, Q. Ouyang, T. Wang, Y. Xie, R. Xu, S. Xue, J. Zhang, L. Zhang, W. Zhao
Institute of High-Energy Physics, Academia Sinica, Beijing, The People's Republic of China[8]

R. Alemany, A.O. Bazarko, G. Bonvicini,[23] M. Cattaneo, P. Comas, P. Coyle, H. Drevermann, R.W. Forty, M. Frank, R. Hagelberg, J. Harvey, P. Janot, B. Jost, E. Kneringer, J. Knobloch, I. Lehraus, E.B. Martin, P. Mato, A. Minten, R. Miquel, Ll.M. Mir,[2] L. Moneta, T. Oest,[31] F. Palla, J.R. Pater,[27] J.-F. Pusztaszeri, F. Ranjard, P. Rensing, L. Rolandi, D. Schlatter, M. Schmelling,[24] O. Schneider, W. Tejessy, I.R. Tomalin, A. Venturi, H. Wachsmuth, A. Wagner, T. Wildish
European Laboratory for Particle Physics (CERN), 1211 Geneva 23, Switzerland

Z. Ajaltouni, A. Barrès, C. Boyer, A. Falvard, P. Gay, C . Guicheney, P. Henrard, J. Jousset, B. Michel, S. Monteil, J-C. Montret, D. Pallin, P. Perret, F. Podlyski, J. Proriol, J.-M. Rossignol
Laboratoire de Physique Corpusculaire, Université Blaise Pascal, IN^2P^3-CNRS, Clermont-Ferrand, 63177 Aubière, France

T. Fearnley, J.B. Hansen, J.D. Hansen, J.R. Hansen, P.H. Hansen, B.S. Nilsson, A. Wäänänen
Niels Bohr Institute, 2100 Copenhagen, Denmark[9]

A. Kyriakis, C. Markou, E. Simopoulou, I. Siotis, A. Vayaki, K. Zachariadou
Nuclear Research Center Demokritos (NRCD), Athens, Greece

A. Blondel, G. Bonneaud, J.C. Brient, P. Bourdon, A. Rougé, M. Rumpf, A. Valassi,[6] M. Verderi, H. Videau[21]
Laboratoire de Physique Nucléaire et des Hautes Energies, Ecole Polytechnique, IN^2P^3-CNRS, 91128 Palaiseau Cedex, France

D.J. Candlin, M.I. Parsons
Department of Physics, University of Edinburgh, Edinburgh EH9 3JZ, UK[10]

E. Focardi,[21] G. Parrini
Dipartimento di Fisica, Università di Firenze, INFN Sezione di Firenze, 50125 Firenze, Italy

M. Corden, C. Georgiopoulos, D.E. Jaffe
Supercomputer Computations Research Institute, Florida State University, Tallahassee, FL 32306-4052, USA [13,14]

A. Antonelli, G. Bencivenni, G. Bologna,[4] F. Bossi, P. Campana, G. Capon, D. Casper, V. Chiarella, G. Felici, P. Laurelli, G. Mannocchi,[5] F. Murtas, G.P. Murtas, L. Passalacqua, M. Pepe-Altarelli
Laboratori Nazionali dell'INFN (LNF-INFN), 00044 Frascati, Italy

L. Curtis, S.J. Dorris, A.W. Halley, I.G. Knowles, J.G. Lynch, V. O'Shea, C. Raine, P. Reeves, J.M. Scarr, K. Smith, I. ten Have, A.S. Thompson, F. Thomson, S. Thorn, R.M. Turnbull
Department of Physics and Astronomy, University of Glasgow, Glasgow G12 8QQ, UK[10]

U. Becker, C. Geweniger, G. Graefe, P. Hanke, G. Hansper, V. Hepp, E.E. Kluge, A. Putzer, B. Rensch, M. Schmidt, J. Sommer, H. Stenzel, K. Tittel, S. Werner, M. Wunsch
Institut für Hochenergiephysik, Universität Heidelberg, 69120 Heidelberg, Germany[16]

D. Abbaneo, R. Beuselinck, D.M. Binnie, W. Cameron, P.J. Dornan, A. Moutoussi, J. Nash, J.K. Sedgbeer, A.M. Stacey, M.D. Williams
Department of Physics, Imperial College, London SW7 2BZ, UK[10]

G. Dissertori, P. Girtler, D. Kuhn, G. Rudolph
Institut für Experimentalphysik, Universität Innsbruck, 6020 Innsbruck, Austria[18]

C.K. Bowdery, P. Colrain, G. Crawford, A.J. Finch, F. Foster, G. Hughes, T. Sloan, E.P. Whelan, M.I. Williams
Department of Physics, University of Lancaster, Lancaster LA1 4YB, UK[10]

A. Galla, A.M. Greene, K. Kleinknecht, G. Quast, B. Renk, E. Rohne, H.-G. Sander, P. van Gemmeren, C. Zeitnitz
Institut für Physik, Universität Mainz, 55099 Mainz, Germany[16]

J.J. Aubert,[21] A.M. Bencheikh, C. Benchouk, A. Bonissent,[21] G. Bujosa, D. Calvet, J. Carr, C. Diaconu, F. Etienne, N. Konstantinidis, P. Payre, D. Rousseau, M. Talby, A. Sadouki, M. Thulasidas, K. Trabelsi
Centre de Physique des Particules, Faculté des Sciences de Luminy, IN^2P^3-CNRS, 13288 Marseille, France

I. Abt, R. Assmann, C. Bauer, W. Blum, H. Dietl, F. Dydak,[21] G. Ganis, C. Gotzhein, K. Jakobs, H. Kroha, G. Lütjens, G. Lutz, W. Männer, H.-G. Moser, R. Richter, A. Rosado-Schlosser, S. Schael, R. Settles, H. Seywerd, R. St. Denis, W. Wiedenmann, G. Wolf
Max-Planck-Institut für Physik, Werner-Heisenberg-Institut, 80805 München, Germany[16]

J. Boucrot, O. Callot, A. Cordier, M. Davier, L. Duflot, J.-F. Grivaz, Ph. Heusse, M. Jacquet, D.W. Kim,[19] F. Le Diberder, J. Lefrançois, A.-M. Lutz, I. Nikolic, H.J. Park,[19] I.C. Park,[19] M.-H. Schune, S. Simion, J.-J. Veillet, I. Videau
Laboratoire de l'Accélérateur Linéaire, Université de Paris-Sud, IN^2P^3-CNRS, 91405 Orsay Cedex, France

P. Azzurri, G. Bagliesi, G. Batignani, S. Bettarini, C. Bozzi, G. Calderini, M. Carpinelli, M.A. Ciocci, V. Ciulli, R. Dell'Orso, R. Fantechi, I. Ferrante, L. Foà,[1] F. Forti, A. Giassi, M.A. Giorgi, A. Gregorio, F. Ligabue, A. Lusiani, P.S. Marrocchesi, A. Messineo, G. Rizzo, G. Sanguinetti, A. Sciabà, P. Spagnolo, J. Steinberger, R. Tenchini, G. Tonelli,[26] C. Vannini, P.G. Verdini, J. Walsh
Dipartimento di Fisica dell'Università, INFN Sezione di Pisa, e Scuola Normale Superiore, 56010 Pisa, Italy

A.P. Betteridge, G.A. Blair, L.M. Bryant, F. Cerutti, J.T. Chambers, Y. Gao, M.G. Green, T. Medcalf, P. Perrodo, J.A. Strong, J.H. von Wimmersperg-Toeller
Department of Physics, Royal Holloway & Bedford New College, University of London, Surrey TW20 OEX, UK[10]

D.R. Botterill, R.W. Clifft, T.R. Edgecock, S. Haywood, P. Maley, P.R. Norton, J.C. Thompson, A.E. Wright
Particle Physics Dept., Rutherford Appleton Laboratory, Chilton, Didcot, Oxon OX11 OQX, UK[10]

B. Bloch-Devaux, P. Colas, S. Emery, W. Kozanecki, E. Lançon, M.C. Lemaire, E. Locci, B. Marx, P. Perez, J. Rander, J.-F. Renardy, A. Roussarie, J.-P. Schuller, J. Schwindling, A. Trabelsi, B. Vallage
CEA, DAPNIA/Service de Physique des Particules, CE-Saclay, 91191 Gif-sur-Yvette Cedex, France[17]

S.N. Black, J.H. Dann, R.P. Johnson, H.Y. Kim, A.M. Litke, M.A. McNeil, G. Taylor
Institute for Particle Physics, University of California at Santa Cruz, Santa Cruz, CA 95064, USA[22]

C.N. Booth, R. Boswell, C.A.J. Brew, S. Cartwright, F. Combley, A. Koksal, M. Letho, W.M. Newton, J. Reeve, L.F. Thompson
Department of Physics, University of Sheffield, Sheffield S3 7RH, UK[10]

A. Böhrer, S. Brandt, V. Büscher, G. Cowan, C. Grupen, G. Lutters, J. Minguet-Rodriguez, F. Rivera,[25] P. Saraiva, L. Smolik, F. Stephan,
Fachbereich Physik, Universität Siegen, 57068 Siegen, Germany[16]

M. Aleppo,[20] M. Apollonio, L. Bosisio, R. Della Marina, G. Giannini, B. Gobbo, G. Musolino, F. Ragusa[20,21]
Dipartimento di Fisica, Università di Trieste e INFN Sezione di Trieste, 34127 Trieste, Italy

J. Rothberg, S. Wasserbaech
Experimental Elementary Particle Physics, University of Washington, WA 98195 Seattle, USA

S.R. Armstrong, L. Bellantoni,[30] P. Elmer, Z. Feng, D.P.S. Ferguson, Y.S. Gao, S. González, J. Grahl, T.C. Greening, J.L. Harton,[28] O.J. Hayes, H. Hu, P.A. McNamara III, J.M. Nachtman, W. Orejudos, Y.B. Pan, Y. Saadi, M. Schmitt, I.J. Scott, V. Sharma,[29] J.D. Turk, A.M. Walsh, Sau Lan Wu, X. Wu, J.M. Yamartino, M. Zheng, G. Zobernig
Department of Physics, University of Wisconsin, Madison, WI 53706, USA[11]

Received: 30 January 1996

Abstract. The electroweak mixing angle is determined with high precision from measurements of the mean difference between forward and backward hemisphere charges in hadronic decays of the Z. A data sample of 2.5 million hadronic Z decays recorded over the period 1990 to 1994 in the ALEPH detector at LEP is used. The mean charge separation between event hemispheres containing the original quark and antiquark is measured for $b\bar{b}$ and $c\bar{c}$ events in subsamples selected by their long lifetimes or using fast D^*'s. The corresponding average charge separation for light quarks is measured in an inclusive sample from the anticorrelation between charges of opposite hemispheres and agrees with predictions of hadronisation models with a precision of 2%. It is shown that differences between light quark charge separations and the measured average can be determined using hadronisation models, with systematic uncertainties constrained by measurements of inclusive production of kaons, protons and Λ's. The separations are used to measure the electroweak mixing angle precisely as
$\sin^2\theta_{\rm w}^{\rm eff} = 0.2322 \pm 0.0008(\text{exp. stat.})$
$\pm 0.0007(\text{exp. syst.}) \pm 0.0008(\text{sep.})$.
The first two errors are due to purely experimental sources whereas the third stems from uncertainties in the quark charge separations.

[1] Now at CERN, 1211 Geneva 23, Switzerland
[2] Supported by Dirección General de Investigación Científica y Técnica, Spain
[3] Now at Dipartimento di Fisica, Università di Lecce, 73100 Lecce, Italy
[4] Also Istituto di Fisica Generale, Università di Torino, Torino, Italy
[5] Also Istituto di Cosmo-Geofisica del C.N.R., Torino, Italy
[6] Supported by the Commission of the European Communities, contract ERBCHBICT941234
[7] Supported by CICYT, Spain
[8] Supported by the National Science Foundation of China
[9] Supported by the Danish Natural Science Research Council
[10] Supported by the UK Particle Physics and Astronomy Research Council
[11] Supported by the US Department of Energy, grant DE-FG0295-ER40896
[12] Also at Supercomputations Research Institute, Florida State University, Tallahassee, USA
[13] Supported by the US Department of Energy, contract DE-FG05-92ER40742
[14] Supported by the US Department of Energy, contract DE-FC05-85ER250000
[15] Permanent address: Universitat de Barcelona, 08208 Barcelona, Spain
[16] Supported by the Bundesministerium für Forschung und Technologie, Germany
[17] Supported by the Direction des Sciences de la Matière, C.E.A.
[18] Supported by Fonds zur Förderung der wissenschaftlichen Forschung, Austria
[19] Permanent address: Kangnung National University, Kangnung, Korea
[20] Now at Dipartimento di Fisica, Università di Milano, Milano, Italy
[21] Also at CERN, 1211 Geneva 23, Switzerland
[22] Supported by the US Department of Energy, grant DE-FG03-92ER40689
[23] Now at Wayne State University, Detroit, MI 48202, USA
[24] Now at Max-Plank-Institüt für Kernphysik, Heidelberg, Germany
[25] Partially supported by Colciencias, Colombia
[26] Also at Istituto di Matematica e Fisica, Università di Sassari, Sassari, Italy
[27] Now at Schuster Laboratory, University of Manchester, Manchester M13 9PL, UK
[28] Now at Colorado State University, Fort Collins, CO 80523, USA
[29] Now at University of California at San Diego, La Jolla, CA 92093, USA
[30] Now at Fermi National Accelerator Laboratory, Batavia, IL 60510, USA
[31] Now at DESY, Hamburg, Germany

1 Introduction

Production of multihadronic events in e^+e^-annihilation is well described by an initial process of $e^+e^- \to q\bar{q}$, followed by gluon radiation and hadronisation. It is expected that the electric charge of particles produced during hadronisation of the initial quark retain some information of its charge [1]. Evidence for such correlations between the charges of produced hadron jets and the parton charge was first observed in neutrino and muon scattering [2]. Jet charge methods are used at LEP in the analysis of electroweak quark asymmetries [3–8], and both integrated [9, 10] and time dependent [11–13] $B^0\overline{B^0}$ mixing measurements. This paper presents the measurement of the forward/backward jet charge asymmetry in an inclusive sample of hadronic Z decays and its interpretation in terms of the electroweak mixing angle $\sin^2\theta_{\rm w}^{\rm eff}$.

The quark charge is estimated by the momentum-weighted hemisphere charge

$$Q_{\rm hem.} = \frac{\sum_{\rm hem.} p_{\|i}^{\kappa} q_i}{\sum_{\rm hem.} p_{\|i}^{\kappa}}, \qquad (1)$$

where q_i is the charge of particle i and $p_{\|i}$ its momentum projected onto the thrust axis. The sum runs over the charged particles in an event hemisphere defined by the thrust axis to be either forward (Q_F) or backward (Q_B) with respect to the incoming electron direction. The parameter κ can be varied from zero to infinity. The best sensitivity is obtained for $\kappa = 1.0$. The choice $\kappa = \infty$ corresponds to the selection of only the leading particle in the hemisphere. The consistency of electroweak measurements upon variation of κ is an important test of the analysis method.

On average the charges of the hemispheres containing the quark, Q_f, and the antiquark, $Q_{\bar{f}}$, in a $q\bar{q}$ event with given flavour, f, differ by the quantity

$$\delta_f = \langle Q_f - Q_{\bar{f}} \rangle, \qquad (2)$$

which is referred to as the charge separation. The difference in the average charge of forward and backward hemispheres of hadronic events

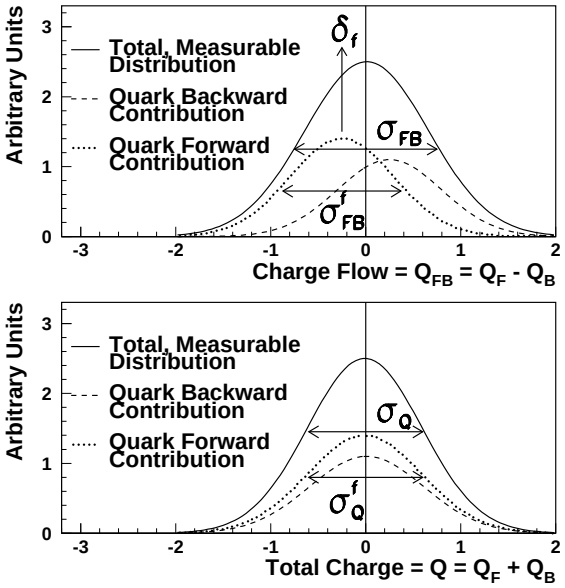

Fig. 1. Illustration of the Q_{FB} and Q charge distributions for a quark of flavour f. The widths of the Q_{FB} and Q distributions in the case the quark f goes forward, σ^f_{FB} and σ^f_Q, are approximately equal if the correlations between hemispheres are small

$$\langle Q_{FB}\rangle \equiv \langle Q_F - Q_B\rangle = A_{acc} \sum_{f=quark\ \ flavours} \delta_f\, A^f_{FB}\, \frac{\Gamma_f}{\Gamma_{had}} \qquad (3)$$

is measured. The acceptance factor, A_{acc} is given by

$$A_{acc} = \frac{4\cos\theta_{max}}{3+\cos^2\theta_{max}}, \qquad (4)$$

where θ_{max} is the polar angle cut on the final state fermions in $e^+e^- \to Z/\gamma \to f\bar{f}$. The value of $\langle Q_{FB}\rangle$ depends on the electroweak asymmetries A^f_{FB} in $e^+e^- \to Z/\gamma \to f\bar{f}$ decays and, with knowledge of the charge separations, is interpreted in terms of the electroweak mixing angle $\sin^2\theta^{eff}_w$. In the analysis below the quantities A^f_{FB}, Γ_f, and Γ_{had} are computed in terms of $\sin^2\theta^{eff}_w$ with ZFITTER [14] and the right hand side of (3) is fit to the measured value of $\langle Q_{FB}\rangle$.

At the Z peak the asymmetry for a quark f may be written as

$$A^f_{FB} = \frac{3}{4}\mathscr{A}_e\mathscr{A}_f \qquad (5)$$

where $\mathscr{A}_e$ is

$$\mathscr{A}_e = \frac{\left(g^e_L\right)^2 - \left(g^e_R\right)^2}{\left(g^e_L\right)^2 + \left(g^e_R\right)^2} \qquad (6)$$

$$\simeq 8\left(0.25 - \sin^2\theta^{eff}_w\right) \qquad (7)$$

and $\mathscr{A}_f$ is similarly defined. The term $\mathscr{A}_e$ is a common factor to all asymmetries in (3). Its relative sensitivity to $\sin^2\theta^{eff}_w$ is an order of magnitude larger than that of $\mathscr{A}_f$. Consequently, the measurement of $\langle Q_{FB}\rangle$ is a sensitive measurement of $\sin^2\theta^{eff}_w$ as defined from the electron couplings [15]. An accuracy of 5% in its measurement results in a determination of $\sin^2\theta^{eff}_w$ with a precision of ± 0.001.

A second element essential to the accuracy of the measurement is that the average charge separation, δ, is directly measurable from data using

$$\bar{\delta}^2 = (\sigma_{FB})^2 - \left(\sigma_Q\right)^2, \qquad (8)$$

where σ_{FB} and σ_Q are the RMS widths of the Q_{FB} and total charge $Q = Q_F + Q_B$ distributions. For a flavour f ($\bar{f}$) the single hemisphere charge measurements, Q_f ($Q_{\bar{f}}$), may be written as

$$Q_f = \langle Q_f\rangle + \mathscr{R}_f \quad \text{and} \quad Q_{\bar{f}} = \langle Q_{\bar{f}}\rangle + \mathscr{R}_{\bar{f}} \qquad (9)$$

where $\mathscr{R}_f$ ($\mathscr{R}_{\bar{f}}$) is the event-by-event fluctuation around the average $\langle Q\rangle_f$ ($\langle Q\rangle_{\bar{f}}$) due to fragmentation. The product of the two hemisphere charges then averages to

$$\langle Q_f Q_{\bar{f}}\rangle = \langle Q_F Q_B\rangle_f = \frac{-\delta^2_f}{4} + \langle \mathscr{R}_f\mathscr{R}_{\bar{f}}\rangle \qquad (10)$$

assuming $\langle Q_f\rangle = -\langle Q_{\bar{f}}\rangle = \delta_f/2$ and using $\langle \mathscr{R}_f\rangle = \langle \mathscr{R}_{\bar{f}}\rangle = 0$. The quantity $\langle \mathscr{R}_f\mathscr{R}_{\bar{f}}\rangle$ arises from correlation between hemisphere charges, by memory of total charge conservation. As illustrated in Fig. 1, the difference in variance of the $(Q_{FB})_f$ and $(Q)_f$ distributions arises from the charge separation δ_f. Expanding (8) for the flavour f and using (10) gives

$$\begin{aligned}\bar{\delta}^2_f &= -4\langle Q_F Q_B\rangle_f - \langle Q_{FB}\rangle^2_f + \langle Q\rangle^2_f \\ &= \delta^2_f - 4\langle \mathscr{R}_f\mathscr{R}_{\bar{f}}\rangle - \langle Q_{FB}\rangle^2_f \\ &= \left[\delta_f(1+k_f)\right]^2. \end{aligned} \qquad (11)$$

Correlations between hemispheres, $\langle \mathscr{R}_f\mathscr{R}_{\bar{f}}\rangle$, are small, and the averages $\langle Q_{FB}\rangle^2_f$ and $\langle Q\rangle^2_f$ are even smaller. Thus δ_f is equal to δ_f to within a κ-dependent correction factor, k_f, that has a value of about 5% at $\kappa = 1.0$. A rigorous treatment including effects of secondary interactions is given in Appendix A.

The dependence of $\bar{\delta}^2$ on the sample flavour composition is written as

$$\bar{\delta}^2 = \sum_{f=quark\ \ flavours} \mathscr{P}_f\,\bar{\delta}^2_f \qquad (12)$$

where the purity $\mathscr{P}_f$ is the fraction of $Z \to f\bar{f}$ events in the sample. In the absence of event selection biases, $\mathscr{P}_f = \Gamma_f/\Gamma_{had}$. Experimental manipulation of the purity in (12) allows a determination of individual charge separations. Using a lifetime-tagged sample [16] of b quarks, the absolute value of δ_b has been measured [6]. By varying the lifetime-tag cuts, the composition of the sample is altered to enhance the c quark content and the absolute value of δ_c is also extracted. With these measurements of heavy quark charge separations, the average separation for light quarks, δ_{uds}, is derived from $\bar{\delta}$ with a relative precision of 2%.

Separations for individual quark flavours can be directly measured in events for which one hemisphere is tagged and the charge measured in the opposite hemisphere [9]. For example, as shown in Sect. 3.2, events with high momentum D^*'s provide enriched samples of c quarks which are used to measure δ_c, whereas those with high momentum Λ's constrain δ_s.

Determination of the individual light quark separations is difficult because of the lack of an efficient tag discriminating between u, d and s type quarks. The reliability of hadronisation models to predict the differences between them is therefore investigated in Sect. 4. It is shown that only a limited number of general principles, implemented in a simple chain model, are required to reproduce jet charge propagation properties of more sophisticated hadronisation models.

As described in Sect. 4.1, although the charge of a u quark is twice the charge of a d quark, the magnitudes of the charge separations for light quark flavours would be identical if only $u\bar{u}$ and $d\bar{d}$ pairs were produced during hadronisation. This common scale of the separation value depends on resonance production and is tightly constrained by the measured value of δ. The observed differences between light quark separations arise from production of strange particles and formation of baryons during the hadronisation process. There is no experimental access to the contributions of these particles to jet charges; therefore, they must be estimated using fragmentation models (Sect. 4.2). Systematic errors in this estimate are determined by the accuracy with which models can simultaneously describe the value of δ and the production of kaons and baryons. The two models considered have quite different philosophies when producing these particles. As shown in Sect. 4.4, spectra are closely reproduced by the JETSET model [17], while HERWIG [18] fails to reproduce baryon production satisfactorily and gives separations that are different but consistent within a large systematic error. Consequently JETSET is used to determine the value of $\sin^2\theta_{\rm w}^{\rm eff}$ quoted in Sect. 5.

2 Measurement of hadronic jet charges

The data set used for this analysis consists of approximately 2.5 million hadronic Z decays recorded by ALEPH during the period from 1990 to 1994. Centre-of-mass energies in the range $M_Z \pm 3$ GeV/c^2 are available for the measurement of the Z line shape. The ALEPH detector is described in [19] and its performance in [20].

Charged track reconstruction is essential to both the event selection and jet charge determination. The ALEPH tracking system consists of two layers of a double-sided silicon vertex detector (VDET), an Inner Tracking Chamber (ITC) and a Time Projection Chamber (TPC). The VDET single hit resolution is $12\mu m$ at normal incidence for both $r-\phi$ and $r-z$ projections. The ITC provides up to eight $r-\phi$ hits from 16 to 26 cm relative to the beam, down to $|\cos\theta|$ = 0.97, with an average resolution of $150\mu m$. The TPC measures up to 21 three-dimensional points per track at radii between 40 and 171 cm, with an $r-\phi$ resolution of $170\mu m$ and an $r-z$ resolution of $740\mu m$, also down to $|\cos\theta|$ = 0.97. Tracks are reconstructed using the TPC, ITC and VDET. A transverse momentum resolution of $\sigma(1/p_T) = 0.6\times10^{-3}$ (GeV/c)$^{-1}$ is observed for 45 GeV muons. Multiple scattering dominates at low momentum and adds a constant term of 0.005 to $\sigma(p_T)/p_T$.

The TPC track-finding efficiency is studied using Monte Carlo simulation. Simulated data used throughout this study are based on events from the ALEPH HVFL03 generator [21]. This employs a modified set of heavy flavour decay routines in the context of the JETSET (Version 7.3) string fragmentation model with initial state photon radiation determined by DYMU02 [22]. The set of model parameters used for simulation are tuned to ALEPH event shape distributions using the method of [23]. This set of parameters is referred to as a the "reference" set. Particle tracking and detector response are simulated using a GEANT description of ALEPH. Simulated events are reconstructed using the same algorithms as those for the analysis of the data. In hadronic events, 98.6% of tracks that cross at least four pad rows in the TPC are reconstructed successfully. This corresponds to a lower transverse momentum cutoff of about 200 MeV/c. The inefficiency is due to track overlaps and cracks, although the latter are minimised by staggering the edges of TPC sectors. This is verified by scanning and studies of the measured two-track separation [24].

2.1 Experimental analysis

The charged track $Z \to q\bar{q}$ selection [25] requires five or more good tracks, carrying more than 10% of the centre-of-mass energy. Good tracks are defined to have at least 4 TPC hits, $|\cos\theta| < 0.95$ and a minimum distance to the interaction point of less than 10 cm in z and 2 cm in $r-\phi$.

For this analysis, further selection cuts are applied. The thrust axis of the event is reconstructed using charged tracks. To ensure containment of the event, it is required that $|\cos\theta_{\rm thrust}| < 0.9$. The event is then divided into two hemispheres by a plane perpendicular to the thrust axis. The charge in each hemisphere is calculated from (1) using all good tracks having a transverse momentum measured relative to the beam direction greater than 200 MeV/c. The $+z$ axis is defined to lie along the direction of the electron beam. The hemisphere which contains this axis is called the forward hemisphere and the other the backward hemisphere. The charges in the forward and backward hemispheres, Q_F and Q_B, are calculated for each event. These are then used to form the difference, $Q_{FB} = Q_F - Q_B$, sum, $Q = Q_F + Q_B$, and product, $Q_F \times Q_B$. The sample averages and RMS widths for these quantities are the main experimental results of the analysis. The forward-backward symmetric quantities $Q_F \times Q_B$ and Q are used as important measurements of the propagation of quark charge through hadronisation as well as constraints when calculating experimental systematic errors on the electroweak asymmetry.

Since the two photon background in the hadronic sample is less than 0.3% and does not affect $\langle Q_{FB}\rangle$ by more than 0.3% of its value, it is neglected in this analysis [3]. The contamination of tau events is 0.2% in the standard hadronic selection [25] which induces a shift of only $0.66\,(\pm0.51)\times10^{-4}$ to $\langle Q_{FB}\rangle$, and is neglected in this analysis.

The analysis is performed using several values of the parameter κ in the range $0.3 \le \kappa \le \infty$. Measured values of $\langle Q_{FB}\rangle$, $\langle Q\rangle$ and $\bar{\delta}$ (determined from (8)) are shown in Table 1 together with Monte Carlo expectations for the charge symmetric quantities $\langle Q\rangle$ and δ. The effects of the data/Monte Carlo discrepancy in $\langle Q\rangle$ will be discussed in Sect. 2.2.2. Correlations between measurements using different κ values are given for $\langle Q_{FB}\rangle$ in Table 22 and for δ in Table 20 in Appendix B.

2.2 Experimental systematic uncertainties

Experimental systematic errors arise from false asymmetries in the detector and event reconstruction, or from differences in particle tracking between data and simulated events. Consequently, systematic uncertainties on measured quantities from the following sources are studied :

Table 1. Measurement results for various values of κ, and Monte Carlo prediction for the reference values of parameters. The first errors are statistical and the second are systematic. The measured values are averaged over all centre-of-mass energies. Errors due to the model of hadronisation are not included here

	Measured values			MC prediction	
κ	$\langle Q_{FB}\rangle \times 10^4$	$\langle Q\rangle \times 10^4$	$\bar{\delta} \times 10^4$	$\langle Q\rangle \times 10^4$	$\bar{\delta} \times 10^4$
0.3	$-43.9 \pm 2.2 \pm 2.4$	$70.6 \pm 1.8 \pm 18.2$	$2077 \pm 4 \pm 51$	118.9 ± 1.7	1995 ± 4
0.5	$-57.6 \pm 2.6 \pm 2.7$	$64.7 \pm 2.1 \pm 17.3$	$2253 \pm 6 \pm 45$	107.4 ± 2.1	2180 ± 6
1.0	$-89.5 \pm 3.8 \pm 3.9$	$52.9 \pm 3.4 \pm 13.9$	$2899 \pm 10 \pm 38$	87.0 ± 3.3	2859 ± 10
2.0	$-126.2 \pm 5.8 \pm 5.9$	$42.4 \pm 5.3 \pm 11.9$	$3718 \pm 18 \pm 39$	72.2 ± 5.2	3721 ± 18
∞	$-145.9 \pm 9.2 \pm 11.8$	$38.1 \pm 8.8 \pm 15.1$	$4357 \pm 41 \pm 49$	71.2 ± 8.6	4421 ± 40

Table 2. Breakdown of systematic error calculation for $\langle Q_{FB}\rangle$, $\langle Q\rangle$, and $\bar{\delta}$, for κ = 1. "Uncorrelated" systematic errors indicate the error on each quantity separately. If $\langle Q_{FB}\rangle$ and $\bar{\delta}$ are used together in the fit of $\sin^2\theta_w^{eff}$ the detector acceptance and resolution systematic uncertainties cancel so that this component of the systematic error is indicated by "correlated"

Source	$\Delta\langle Q_{FB}\rangle$ $\times 10^4$	$\Delta\langle Q\rangle$ $\times 10^4$	$\Delta\bar{\delta}$ $\times 10^4$
Biases in track reconstruction			
–tracks with high transverse impact parameters	1.6	3.9	9.7
–tracks with high longitudinal impact parameters	0.7	1.4	1.5
–tracks at low angles	2.1	2.5	4.7
–tracks with few TPC hits	2.8	12.9	6.8
–tracks with anomalously high momentum	0.5	0.5	1.4
Biases in momentum reconstruction	0.3	1.5	0.0
Secondary interactions (from A_{mat})	0.1	–	–
Uncorrelated $\langle Q_{FB}\rangle$ and $\bar{\delta}$	3.9	13.9	12.9
Secondary interactions ($\varepsilon_f - \varepsilon_{\bar{f}}$)	1.1	–	34.1
Detector acceptance and resolution	0.4	–	11.6
Correlated $\langle Q_{FB}\rangle$ and $\bar{\delta}$	1.2	–	36.0
Total experimental systematic uncertainty:	4.0	13.9	38.3

– sign or polar angle biases in track reconstruction;
– momentum reconstruction biases;
– secondary interactions in and before the tracking system;
– detector acceptance and resolution.

The breakdown of systematic errors from these sources is summarised in Table 2 for κ = 1. Methods used to determine the systematic errors represent an update of those described in [3] for $\langle Q_{FB}\rangle$ and are extended to the quantities $\langle Q\rangle$ and $\bar{\delta}$.

2.2.1 Biases in track and momentum reconstruction. Significant asymmetries can arise if tracks from particles having positive charge are reconstructed with different efficiencies from those coming from particles with negative charge. Badly reconstructed tracks tend to be at low angles, have few hits, anomalously high momenta or large impact parameters. The contribution of these tracks to $\langle Q_{FB}\rangle$, $\bar{\delta}$ and $\langle Q\rangle$ is measured by removing tracks close to the acceptance cuts, recomputing the thrust axis, and comparing this new jet charge event-by-event with the original value. As the cuts are varied, the largest of either the systematic difference between data and Monte Carlo or the statistical accuracy of the difference is taken as the systematic error. The method is shown to be robust against the magnitudes of the cut variations and whether or not the thrust axis is recomputed with each change of cuts.

Momentum biases can play an important role in the jet charge determination. Momentum scale biases are corrected for each charge sign and track angle using a sample of collinear $Z \to \mu^+\mu^-$ events. A systematic error corresponding to 50% of the effect of applying the corrections is assigned to all measured quantities.

The effects of systematic errors in tracking on $\bar{\delta}$ are studied using the distribution of event-by-event differences in $Q_F \times Q_B$ (11) before and after badly reconstructed tracks have been removed. In the determination of $\langle Q\rangle$ these are the only important systematic effects. The measured value of $\langle Q\rangle$ with this systematic error is used extensively for determining the remaining components of the systematic error in $\bar{\delta}$ and $\langle Q_{FB}\rangle$.

2.2.2 Secondary interactions in detector material. Three effects from secondary interactions are considered. First, asymmetries in the nuclear cross sections for particles and antiparticles can give different amounts of additional charge to jets originating from quarks than for jets originating from antiquarks. A second effect is that the amount of material in the detector may be forward/backward asymmetric with respect to the interaction point. Finally, the detector material may dilute the overall charge because high momentum particles carrying a large weight in the jet charge defined in (1) interact and produce a number of lower momentum particles which carry less weight. The impact of these effects is described in detail in Appendix A where the main results for a single flavour are

$$\langle Q_{FB}\rangle_f^{det} = \langle Q_F - Q_B\rangle_f^{det} = A_{FB}^f \left(\delta_f^{gen} + \varepsilon_f - \varepsilon_{\bar{f}}\right) + A_{mat}\left(\varepsilon_f + \varepsilon_{\bar{f}}\right) \quad (13)$$

$$\left(\bar{\delta}_f^{det}\right)^2 = \left(\delta_f^{gen} + \varepsilon_f - \varepsilon_{\bar{f}}\right)^2 - \left(\langle Q_{FB}\rangle_f^{det}\right)^2 + \langle \mathscr{R}_f^{det}\mathscr{R}_{\bar{f}}^{det}\rangle \quad (14)$$

$$\langle Q\rangle^{det} = \langle Q_F + Q_B\rangle_f^{det} \simeq \varepsilon_f + \varepsilon_{\bar{f}} \quad (15)$$

where the material asymmetry in the detector is denoted by A_{mat}. Additional charge from the detector modifies the charge in the hemisphere containing the quark (antiquark) by an amount ε_f ($\varepsilon_{\bar{f}}$). The labels *gen* and *det* are explicitly written to distinguish the quantities with and without detector effects.

For a single quark flavour it is evident that in a measurement of A_{FB}^f from $\langle Q_{FB}\rangle_f$ and δ_f, the effects of cross section asymmetries cancel because the charge separation, δ_f^{det} =

$\left(\delta_{\rm f}^{\rm gen} + \varepsilon_{\rm f} - \varepsilon_{\bar{\rm f}}\right)$, appears in both (13) and (14). Since the desired quantity to be measured is A_{FB}^{f}, the only unknown quantities in (13), (14), and (15) are A_{mat} and $\langle \mathscr{R}_{\rm f}^{\rm det} \mathscr{R}_{\bar{\rm f}}^{\rm det} \rangle$. The value of A_{mat} and its associated systematic uncertainty are determined from a comparison of photon conversions in data and Monte Carlo. The hemisphere correlations $\langle \mathscr{R}_{\rm f}^{\rm det} \mathscr{R}_{\rm f}^{\rm det} \rangle$ contain no significant contribution from detector effects and are computed from Monte Carlo. Systematic errors are obtained from Monte Carlo variations as described in [6].

In this analysis these equations are summed over all flavours; however, the conclusions concerning a single flavour are unaltered. This is because, as mentioned in Sect. 2.2.3, the strongly interacting components (π, K, baryon) of the jet charge separations for light quarks show a uniform dilution relative to the generated charge in Monte Carlo. For heavy quarks, $\delta_{\rm b}^{\rm det}$ and $\delta_{\rm c}^{\rm det}$ are measured directly.

A correction due to A_{mat} needs to be evaluated when (13), (14) and (15) are used simultaneously to determine $\sin^2\theta_{\rm w}^{\rm eff}$. It is found that $A_{mat} = -0.03 \pm 0.18\%$ and the Monte Carlo prediction is $A_{mat} = -0.09 \pm 0.17\%$. These values are consistent with zero and with each other. Based on the last term in (13) and on (15), a systematic error on Q_{FB} is taken to be the statistical accuracy on the difference between the data and Monte Carlo values of the material asymmetry, ΔA_{mat}, multiplied by the full magnitude of the measured charge: $\Delta\langle Q_{FB}\rangle = \Delta A_{mat} \times \langle Q\rangle$.

When the measurements of $\langle Q_{FB}\rangle$ and δ are quoted independently, it is necessary to assign a systematic uncertainty to the effect of cross section differences in material interactions. As shown in Table 1, the total charge $\langle Q\rangle$ is significantly positive and different from the simulated prediction. The discrepancy between the measured value of $\langle Q\rangle$ between data and Monte Carlo is a measure of the inadequacy of the simulation of secondary interactions. Conservatively, the full amount of the discrepancy is assigned to the difference, $(\varepsilon_{\rm f} - \varepsilon_{\bar{\rm f}})$, as well. This is equivalent to attributing the full discrepancy between $\langle Q\rangle$ in the data and simulation as being entirely due to either quarks or antiquarks.

2.2.3 Detector acceptance and resolution. In addition to the effects of material interactions described in the last section, reconstructed jet charges differ from those computed from all Z decay products because of acceptance losses and detector resolution. Monte Carlo simulation is expected to reproduce these effects. Simulated values of charge separations for various light quark flavours at $\kappa = 1$ are shown in Table 3. Three "levels" are indicated:

(i) generated charged particles with a lifetime longer than 10^{-9} seconds;
(ii) the same, but including decays of K^0's and Λ's plus geometrical acceptance cuts;
(iii) a full simulation of the detector followed by event reconstruction using the same algorithms for the Monte Carlo events as for the data.

In each case, the total charge separation is given in terms of components identified by particle type: $\delta_{\rm f} = \delta_{\rm f}^{\pi} + \delta_{\rm f}^{\rm K} + \delta_{\rm f}^{\rm p} + \delta_{\rm f}^{\rm other}$. The contribution $\delta_{\rm f}^{\rm other}$ includes particles other than protons, pions and kaons: electrons and muons from decays of charged pions and kaons or from semileptonic decays of mesons and baryons containing heavy flavours produced by gluon splitting. In the third level the jet charge is attributed either to particles coming directly from Z decays or to fake tracks and nuclear interactions in the detector material. Fake tracks result from coordinates not used in overlapping real tracks, additional arms of real track helices, or particles recoiling from the calorimeter into the tracking volume. The main dilution is due to detector response and reconstruction. This results in a flavour-independent dilution of $\delta_{\rm f}$ that is the same for pion, kaon, and proton components. There is one exception to this observation. A significant portion of the proton component of the s quark charge separation comes from decays of fast Λ's which contain a primary s quark. The Λ can be lost either because it decays late in the TPC and has less than four coordinates, or if it reaches the calorimeter before decay. As a consequence, the proton component of the s quark charge separation is strongly affected by geometry.

Systematic error contributions from detector acceptance and resolution are due to the understanding of track losses from cracks, overlap between tracks, secondary interactions, and uncertainties in the thrust axis determination. Adequate simulation of cracks is verified using a sample of dilepton events. Simulation of overlaps is tested by studying the two track separation distribution [24]. Track losses become significant for angles between tracks of less than two degrees and are well described by simulation. The total loss of tracks is monitored by scanning events [3] where it is found that less than 0.1% of tracks fail to be reconstructed for reasons other than those simulated in the Monte Carlo. Combining this with an estimated total tracking inefficiency of 1.4% from simulation, indicates that the loss of particles due to tracking is known to better than 8% of its value. Therefore, a systematic error of 8% of the 5% difference between the second and third levels in Table 3 is assigned to take into account possible overall inadequacies of the simulation of cracks and overlaps.

Uncertainties in the thrust axis determination lead to assignment of tracks to the wrong hemisphere. This is studied [20] by comparing results obtained with the thrust axis reconstructed from the full energy flow data and that from charged tracks only. The difference in charge separations is not statistically significant, remaining below 1% for all flavours and values of κ. This indicates that thrust axis uncertainties are negligible on average.

3 Jet charges from heavy flavour decays of the Z

This section describes the experimental determination of charge separations for heavy flavour quarks. The analysis to obtain $\delta_{\rm b}$ is described in [6] and extended to obtain $\delta_{\rm c}$. A second analysis to obtain $\delta_{\rm c}$ is performed using a D^* tag. The two methods are compared to each other and to a computation of $\delta_{\rm c}$ obtained from Monte Carlo using measured inclusive branching ratios.

Table 3. Charge separations for κ = 1 at three levels of simulation, for the reference values of Monte Carlo parameters. The first step, "generated," uses all generated charged particles with lifetime longer than 10^{-9} seconds. The second step, "generated + geometry," decays K^0's and Λ's and removes particles that would fail cuts in transverse momentum and angular acceptance. The third step, "full simulation," includes all detector effects and reconstruction. For the final step the particles are further discriminated according to whether they come from the hadronic event, a nuclear interaction in the detector material and fake tracks from coordinates not used in overlapping tracks, additional spirals of helices of real tracks or particles recoiling back from the calorimeter into the tracking volume

u quark separation					
	Generated	Generated + geometry	Full simulation		
			Total	Hadronic event	Fakes & interactions
Total	+0.4308 ±0.0018	+0.4316	+0.4188 ±0.0008	+0.4104	+0.0084
Pions	+0.2898 ±0.0016	+0.2913	+0.2792 ±0.0007	+0.2773	+0.0019
Kaons	+0.0654 ±0.0008	+0.0657	+0.0630 ±0.0004	+0.0628	+0.0002
Protons	+0.0757 ±0.0008	+0.0747	+0.0702 ±0.0003	+0.0689	+0.0013
Other	−0.0001 ±0.0001	−0.0001	+0.0064 ±0.0001	+0.0014	+0.0050
d quark separation					
	Generated	Generated + geometry	Full simulation		
			Total	Hadronic event	Fakes & interactions
Total	−0.2368 ±0.0016	−0.2384	−0.2302 ±0.0007	−0.2264	−0.0037
Pions	−0.2800 ±0.0014	−0.2802	−0.2668 ±0.0006	−0.2649	−0.0019
Kaons	+0.0345 ±0.0007	+0.0342	+0.0330 ±0.0003	+0.0329	+0.0001
Protons	+0.0087 ±0.0007	+0.0077	+0.0075 ±0.0003	+0.0070	+0.0005
Other	−0.0000 ±0.0001	−0.0000	−0.0038 ±0.0001	−0.0014	+0.0024
s quark separation					
	Generated	Generated + geometry	Full simulation		
			Total	Hadronic event	Fakes & interactions
Total	−0.2894 ±0.0015	−0.3067	−0.3069 ±0.0007	−0.3023	−0.0045
Pions	−0.0479 ±0.0013	−0.0487	−0.0463 ±0.0006	−0.0455	−0.0008
Kaons	−0.2880 ±0.0011	−0.2883	−0.2732 ±0.0005	−0.2724	−0.0008
Protons	+0.0467 ±0.0007	+0.0304	+0.0204 ±0.0003	+0.0200	−0.0004
Other	−0.0001 ±0.0001	−0.0001	−0.0077 ±0.0001	−0.0044	−0.0033

3.1 Measurement of δ_c and δ_b using a lifetime tag

The analysis is a modified form of that used to determine δ_b for the measurement of A_{FB}^b by jet charge [6]. The value of δ defined in (12) is measured in a series of increasingly pure $b\bar{b}$ samples selected with the lifetime tag algorithm [16]. The flavour composition of the data sample varies depending on the cut on the probability calculated from the observed lifetime that a hemisphere contains a b quark. The flavour purities in (12) are separated into those for light quarks, $\mathscr{P}_{uds}$ and heavy flavours, $\mathscr{P}_c$ and $\mathscr{P}_b$ and their dependency on the lifetime cut is determined as described in [16]. The data for δ are shown as a function of b-purity in Fig. 2a and purities for light and c quarks are shown as a function of that for b quarks in Fig. 2b. The relative contributions of quark charges to a measurement of δ are varied using lifetime cuts and a fit of δ_{uds}, δ_c, and δ_b to δ is performed. Measurements of δ shown in Fig. 2a make use of only 1991 − 1993 data.

Measurements of heavy flavour charge separations are corrected for the bias introduced by the lifetime tag and include both statistical and systematic errors as evaluated in [6]. It is important to note that light flavours are assumed to tag with equal efficiencies. This is known [6] not to be exactly true, especially for severe lifetime tag selections, and thus represents a source of systematic uncertainty in the interpretation of light quark constraints. Uncertainties from light and $c\bar{c}$ quark purities are propagated through to the values of δ which are used in the fit.

Table 4. The corrections k_f in percent for u, d, s, c and b quarks for various κ values. The combined statistical and systematic error is given

κ	u	d	s	c	b
0.3	15.3 ± 2.5	30.8 ± 4.4	26.6 ± 3.5	15.4 ± 2.7	36.4 ± 3.6
0.5	8.6 ± 1.1	14.8 ± 3.3	11.6 ± 2.3	8.5 ± 2.5	18.4 ± 2.3
1.0	5.5 ± 1.2	4.7 ± 1.9	5.4 ± 1.1	2.2 ± 1.1	8.9 ± 1.1
2.0	5.3 ± 1.0	3.7 ± 1.8	4.9 ± 1.2	1.2 ± 3.6	8.1 ± 1.8
∞	5.8 ± 1.3	4.7 ± 3.8	5.1 ± 1.8	0.0 ± 8.8	6.5 ± 3.6

Values for k_f in (11) are extracted from Monte Carlo simulation. It is shown in [6] that such corrections are small and relatively insensitive to hadronisation model parameters. The latter is difficult to check with high precision due to limited Monte Carlo statistics and remains the dominant uncertainty of the method. The relative correction terms, k_f, for f = u, d, s, c and b quarks given in Table 4 are obtained using the full ALEPH detector simulation. The corrections assume the forward-backward asymmetries and $\langle Q_f \rangle$ values inherent in the simulation with systematic errors as calculated in [6]. The extracted values of δ_b and δ_c using this method are given in Table 5.

3.2 Measurement of δ_c using a $D^{*\pm}$ tag

The principle of this method is to select events enhanced in c quarks based on the presence of a high momentum $D^{*\pm}$ in one hemisphere. The charge of the $D^{*\pm}$ is used to tag the charge in the opposite hemisphere Q_{opp}.

Table 5. Absolute values of δ_c from the fit to $\bar{\delta}$, extracted values of δ_c from the combined sample of $D^{*\pm}$ events and absolute values of δ_b from the fit to $\bar{\delta}$. The final values of δ_c and δ_b shown in the last two rows are obtained from a combined fit of the above results. Errors represent total statistical and systematic uncertainties

κ	0.3	0.5	1.0	2.0	∞
$\lvert\delta_c\rvert$ from lifetime	0.186 ± 0.012	0.200 ± 0.015	0.222 ± 0.028	0.222 ± 0.056	0.001 ± 0.263
δ_c from D^*	0.195 ± 0.011	0.199 ± 0.013	0.193 ± 0.020	0.175 ± 0.030	0.166 ± 0.034
$\lvert\delta_b\rvert$ from lifetime	0.112 ± 0.004	0.142 ± 0.004	0.210 ± 0.007	0.291 ± 0.011	0.352 ± 0.014
$\lvert\delta_c\rvert$ combined fit	0.192 ± 0.009	0.200 ± 0.010	0.211 ± 0.016	0.208 ± 0.026	0.194 ± 0.035
$\lvert\delta_b\rvert$ combined fit	0.114 ± 0.004	0.141 ± 0.004	0.208 ± 0.006	0.288 ± 0.011	0.365 ± 0.014

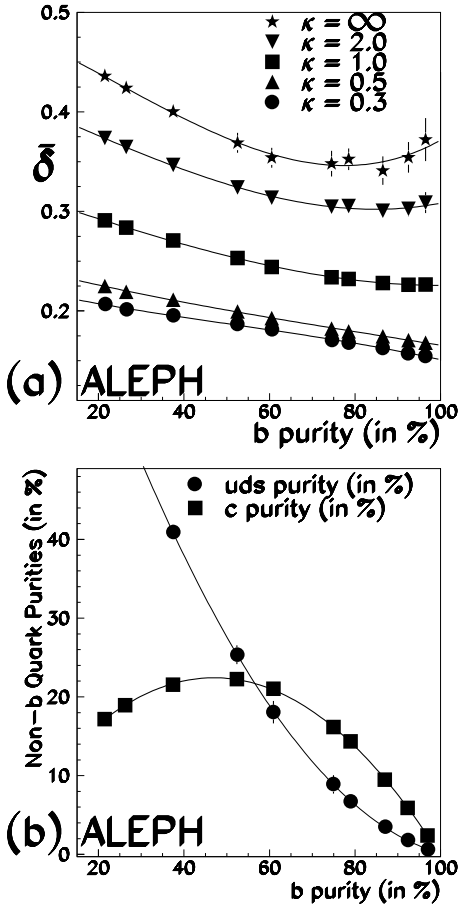

Fig. 2. (a) Measured values of $\bar{\delta}$ are plotted as a function of b purity. Results are shown for a variety of κ values. **(b)** Light (u, d, s) and c quark purities as a function of the b purity $\mathscr{P}_b$. The curves are parameterisations

The analysis begins with a selection of $D^{*\pm}$ samples as explained in [26]. Three decay modes are used, yielding a total of 9208 selected $D^{*\pm}$ candidates. The charge in the hemisphere opposite a D^{*+} candidate may be written

$$\langle Q_{opp}^{D*} \rangle = \frac{1}{1 - f_{background}} \langle Q_{opp}^{D*} \rangle_{measured} - \frac{f_{background}}{1 - f_{background}} \langle Q_{opp}^{D*} \rangle_{background} \quad (16)$$

where $f_{background}$ is the fraction of background under the signal as estimated in [26], $\langle Q_{opp}^{D*} \rangle_{measured}$ is the measured charge in the hemisphere opposite the D^{*+}, and $\langle Q_{opp}^{D*} \rangle_{background}$ is the background jet charge. This background charge is estimated from sidebands of the D^*-D mass difference distributions and found to be consistent with zero for most values of κ. At the largest κ values there is a small excess; however, in all cases, the statistical error on the background charge or the charge itself is insignificant relative to the statistical error on the observed hemisphere charge. Therefore, the main effect of the background is to dilute the charge from heavy flavours.

The charm fraction in the sample remaining after background subtraction is estimated in [26] to be $f_c = 79 \pm 3\%$. The fraction is independent of the selected decay mode within the quoted experimental uncertainty. The $c\bar{c}$ and $b\bar{b}$ contributions to the corrected hemisphere charge $\langle Q_{opp}^{D*} \rangle$ in (16) may be written as

$$\langle Q_{opp}^{D*\pm} \rangle = \mp \frac{1}{2} [f_c (\delta_c - \xi_c) + (1 - f_c)(1 - 2\chi_{eff})(\delta_b - \xi_b)] \quad (17)$$

where δ_b is that provided in Sect. 3.1. The selection of a high momentum $D^{*\pm}$ biases the heavy flavour charge separations by ξ_c and ξ_b. The value of ξ_c is 50% of the statistical error on δ_c and ξ_b has an effect that is an order of magnitude smaller than that of ξ_c. The probability, in a $b\bar{b}$ event containing a $D^{*\pm}$, that a D^{*-} came from the b quark is $\chi_{eff} = 0.177 \pm 0.041$. It is computed from mixing measurements and branching ratios in [26] and amounts to a correction whose magnitude is the same as the statistical error. Values of δ_c are extracted by solving (17) using the combined values of $\langle Q_{opp}^{D*} \rangle$ and are given in Table 5. The errors are statistically dominated; the largest systematic error arises from knowledge of f_c, and uncertainties in $f_{background}$, δ_b, χ_{eff}, ξ_c and ξ_b are negligible.

3.3 Combined $D^{*\pm}$ and lifetime tag charge separation measurements

The two measurements of δ_c presented here are complementary in that the $D^{*\pm}$ analysis indicates both the sign and magnitude of δ_c, whereas lifetime measurements only give the absolute value. The values obtained from the two methods are plotted as a function of κ in Fig. 3a. Since there is good agreement, the results are combined by performing a global fit using correlations derived from the two measurements and for κ in the range $0.3 \leq \kappa \leq \infty$. The quantity f_c is allowed to float in the fit within its error. The results of the combined fit are given in Table 5. The task of combining results is complicated by correlations between measurements of δ_c for various κ values, between measurements of δ_b for various κ values, and between δ_c and δ_b from the lifetime

tag, all of which are obtained from data. Additional correlations between δ_c from $D^{*\pm}$ and (δ_c, δ_b) from the lifetime tag arise from the small overlap in data samples. The effect of this is conservatively estimated by studying how many of the selected $D^{*\pm}$ events are present in the lifetime tag fits used in [6].

Since charmed mesons and baryons carry a large fraction of the beam momentum, tracks coming from these particles determine the δ_c value. After describing the charmed meson and baryon spectra using the Peterson fragmentation function [27] as implimented in JETSET with the parameter $\epsilon_c = -0.05$, a vector to pseudoscalar ratio $V/(V+PS) = 0.6$ for c quarks and no tensor production, the charm charge separation shows a further sensitivity to knowledge of the various D branching ratios. A JETSET Monte Carlo computation of δ_c is shown in Fig. 3a and is in agreement with the experimental determination. This computation reproduces the measurement only when D inclusive branching ratios to kaons and leptons introduced in the Monte Carlo are in agreement with data [28]. The measured values of δ_b are compared to the JETSET Monte Carlo computation in Fig. 3b with $\epsilon_b = -0.0045$, a vector to pseudoscalar ratio $V/(V + PS) = 0.6$ for b quarks and no tensor production.

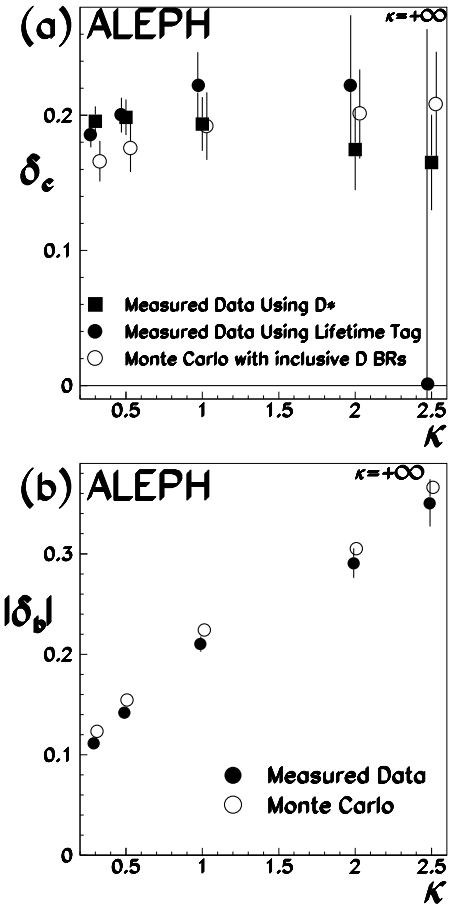

Fig. 3. (a) Comparisons of the lifetime tag and $D^{*\pm}$ measurements of δ_c and with that expected from Monte Carlo simulation. **(b)** Comparison of the lifetime tag measurement of δ_b with that expected from Monte Carlo simulation

4 Charge separations for light quarks

Unlike heavy quarks c and b which can be readily tagged, the light quarks u, d and s are essentially indistinguishable from each other. The only experimental constraint on their charge separations is the global measurement of $\bar{\delta}$. This global measurement is quite sensitive to effects that would multiply the quark separations by a common scale factor, but, because of the different signs of charge separations, it is relatively insensitive to additive contributions. Unfortunately, because all forward-backward asymmetries at the Z pole have the same sign, the extraction of $\sin^2\theta_w^{\rm eff}$ from $\langle Q_{FB}\rangle$ is quite sensitive to such effects.

This problem can be described mathematically by writing the charge separations in terms of a common jet charge δ_0 and individual deviations from it:

$$\delta_f = \frac{q_f}{|q_f|}\delta_0 + \Delta_f \tag{18}$$

where q_f is the quark charge. Using a first order expansion in (Δ_f/δ_0) in (3) and (12) to form the ratio of $\langle Q_{FB}\rangle$ and $\bar{\delta}$ yields

$$\frac{\langle Q_{FB}\rangle}{\bar{\delta}} \simeq \langle A_{FB}\rangle + \left(1 - \langle A_{FB}\rangle\right)\sum_{f=1}^{5}\mathscr{P}_f\frac{\Delta_f}{\delta^0}, \tag{19}$$

where

$$\langle A_{FB}\rangle = A_{acc}\sum_{f=1}^{5}A_{FB}^f\frac{q_f}{|q_f|}\mathscr{P}_f, \tag{20}$$

and A_{acc} is defined in (4). For the quark mixture, the asymmetry correction term is proportional to the sum of the deviations from the average value. The value of Δ_f/δ_0 being typically 25%, the correction term is not small and generates sensitivity to fragmentation effects.

The determination of the light quark separations performed in this section begins by an examination of the sources of differences between them. It is found that the correction terms Δ_f would be zero if the fragmentation process would produce only light mesons composed of u and d quarks. Non-zero values arise from kaon and baryon production, which can be described using two different fragmentation models, JETSET and HERWIG. From them the light quark charges are derived. Systematic errors are determined by the degree of accuracy with which the models are capable of simultaneously describing the measurements of δ and the production of kaons and baryons in hadronic Z decays.

4.1 Sources of differences between light quark charge separations

An examination of the results of the JETSET fragmentation model shown in Table 3 leads to the following conclusions:

1. Before accounting for nuclear interactions with the detector and reconstruction effects, the charge separations are +0.43, -0.24, and -0.29, for u, d and s quarks. They

have the same sign as the quark charges. Approximating $\bar{\delta}_{\rm uds}$ as

$$\bar{\delta}^2_{\rm uds} \simeq \sum_{\rm f=uds} \frac{\Gamma_{\rm f}}{\Gamma_{\rm had}} \delta^2_{\rm f}, \tag{21}$$

neglects the small contributions from $\mathscr{R}_{\rm f}$, $\langle {\rm Q}^{\rm f}_{\rm FB}\rangle^2$ and $\langle {\rm Q}^{\rm f}\rangle^2$. The differences, $\Delta_{\rm f}$, of light quark separations from the value of $\left|\bar{\delta}_{\rm uds}\right| \simeq 0.32$ are all positive, the largest one being 0.10 for the u quark.

2. The largest contribution to u and d quark jet charges comes from pions whereas the largest contribution to the s quark jet charge comes from kaons. The value of this component is the same for all three quarks and quite close to the value of $\bar{\delta}_{\rm uds}$.
3. There are differences both in sign and magnitude between the smaller components from kaons for u, d quarks (or pions for s quarks) and from baryons. These particles are responsible for the different charge separations between quarks.
4. In the case of s quarks, the baryon contribution is dominated by Λ's. The momentum weighting in the $\Lambda \to p\pi^-$ decay leads to a positive charge contribution. This component is the most affected by detector acceptance effects.

The fact that $\delta^\pi_u = -\delta^\pi_d$ is a consequence of the Gell-Mann Nishijima equation ([29]):

$$Q = T_3 + \frac{Y}{2} \tag{22}$$

where Y is the sum of baryon number, strangeness, charm and beauty. Under interchange of u and d quarks, i.e. $T_3 \to -T_3$, then $Q \to -Q$ if and only if the hypercharge is zero, which is the case for mesons made of u and d quarks: pions and other mesons decaying exclusively into pions.

This symmetry and the equality with δ^K_s can easily be seen diagrammatically from the first two lines of Fig. 4. This figure represents the first step in the fragmentation process, where the leading quark is associated with an antiquark originating from the breaking of the colour flux. As indicated in the first two lines, the probability f_u that the antiquark is a $\bar{u}$ quark is assumed to be the same as for a d quark and the symmetry is evident.

In the third line of Fig. 4 the colour flux is broken by an $s\bar{s}$ pair with probability $f_s < f_u$ and the leading quark is combined with an $\bar{s}$. The symmetry is broken, the u quark receiving an additional positive charge from a K^+, the d and s quarks a zero charge from a K^0 or η. This can be related to (22) with kaons having a hypercharge of 1. Since the rest of the fragmentation chain is the same for all three quarks, this first step determines the differentiation of the charge separations.

The case of baryons is similar. If the primary quark is associated with a pair of quarks originating from successive breaking of the colour flux, (or from the breaking of the colour flux into a diquark pair), the symmetry between the three quark flavours is broken again as shown in Fig. 5. This is related to the nonzero hypercharge of baryons. Fragmentation of a u quark receives a large positive contribution from protons, while d quarks receive a smaller positive contribution. In the case of s quark fragmentation, a sizeable

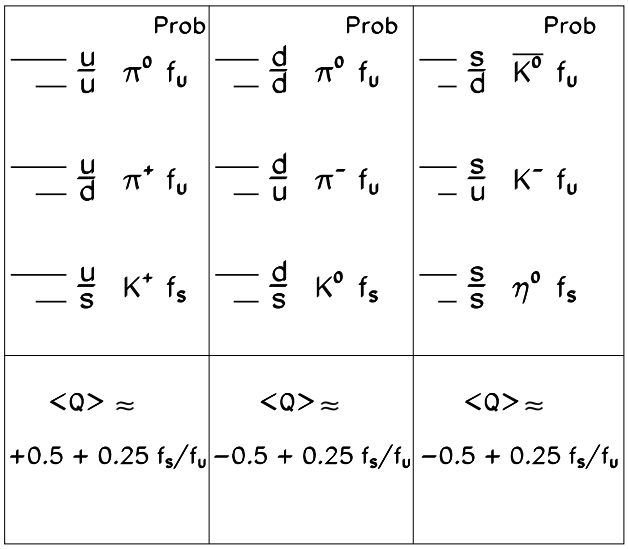

Fig. 4. Illustration of u/d-symmetry and symmetry-breaking due to $s\bar{s}$ pair production for $\kappa \to \infty$, in the case where the leading particle contains the primary quark and when the ratio of the probabilities $f_{\rm s}/f_{\rm u}$ is small

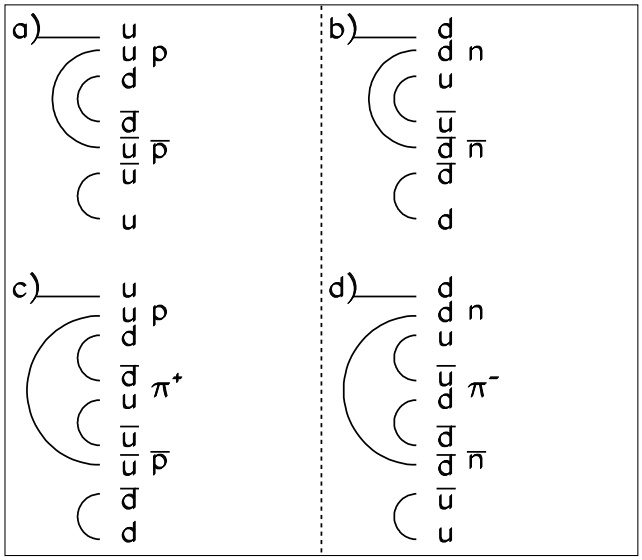

Fig. 5. Illustration of u/d-symmetry-breaking in baryon production. The "popcorn" mechanism is illustrated in **(c)** and **(d)**

production of Λ's is expected, leading to a positive contribution from the proton in the $\Lambda \to p\pi^-$ decay and a small negative contribution from the π^-.

While it is reasonable that kaon production can be adopted from a model of pion production through use of a simple mass scaling, there are several models for baryon production. Two are shown in Fig. 5 and represent different types of quark flow diagrams. Models propose a mechanism [30] where a pion can appear between baryons. The rate at which this phenomenon occurs is described by an additional parameter (the "popcorn" parameter). This effect of this process is to increase the difference in baryon-antibaryon momenta and hence their contribution to the jet charge. At the same time, it decreases the correlation between baryon

and antibaryon, a quantity observed in data from Λ-$\bar{\Lambda}$ correlations.

In these simple examples the resulting value of $\bar{\delta}$ is insensitive to the symmetry-breaking components due to kaons or baryons, and therefore remains a useful test of the basic charge separation.

There is no direct access to the u/d-symmetry-breaking components of charge separation and they are calculated using fragmentation models. However, since pion production dominates by an order of magnitude over kaon and baryon production, the corrections for u/d-symmetry-breaking effects remain at a manageable level. Furthermore, the combination of fitting the inclusive particle spectra and the two particle correlations stringently constrains the fragmentation models.

4.2 Charge separation from fragmentation models

The heuristic arguments developed in the previous section give an explanation for the patterns observed in Table 3. These arguments are based on studies of the first stage of hadronisation. The further development of these arguments involves extending the simple diagrams of Fig. 4 to include the creation of more particles. This is done using a toy model in which the above results are confirmed. The toy model is used only to understand which of the hadronisation model parameters control the charge separations and to guide the quantitative evaluation of systematic errors. After this, sophisticated models such as JETSET and HERWIG are used. The distribution of momenta of particles created and their correlations are considered. This leads finally to a quantitative estimate of charge separations through a simulation of the fragmentation process.

The propagation of charge from the quarks to the final state particles through fragmentation is based on a few simple principles: quantum number conservation, u/d-symmetry and local momentum conservation. The main features of charge propagation can be obtained from a simple model of hadronisation. In this model, a chain of quark pairs is generated according to their probability of production from the vacuum f_u:f_d:f_s = 1:1:γ_s. For each pair the transverse momentum is locally balanced, with a Gaussian distribution having σ = 350 MeV/c. The longitudinal momenta of the newly created meson states are generated according to the Lund Symmetric fragmentation function using the corresponding pion and kaon masses. Study of this model leads to the following observations:

1. If no $s\bar{s}$ pair is produced during fragmentation, the charge separations are only affected by resonances. The s charge differs from the d charge through the change in the identity of the first-rank particle from a pion to a kaon because $m_K > m_\pi$. The symmetry between u and d is preserved.
2. When $s\bar{s}$ pairs are produced, the u/d-symmetry is broken.
3. The value of $\bar{\delta}$ is affected by point 1 and not by point 2.
4. The shapes and means of the jet charge distributions are similar to those obtained with JETSET under conditions where non-strange resonance masses are assigned the pion mass and strange resonances are assigned the kaon mass.

Given the above considerations, the requirements on a fragmentation model for predicting the jet charge separations properly are the following.

(a) Reproduction of the u/d symmetric portion of the charge separation $\bar{\delta}$ for all values of κ. This establishes the degree of accuracy to which the model is capable of describing charge propagation. The main parameters for fixing this property will be resonance production and the longitudinal fragmentation function.
(b) Reproduction of kaon production, both in number and in momentum spectrum. The production of kaon resonances is also an important parameter. An important aspect of the calculation of the contribution of kaons to jet charge is the vicinity in phase space of the two kaons produced by the same $s\bar{s}$ pair, since this will affect how the charge of the second kaon compensates the charge of the first; therefore, kaon correlations need to be reproduced adequately.
(c) Reproduction of baryon production, in number and momentum spectrum. A proper description of baryon correlations is important because of the possibility that in addition to the fragmentation function additional dynamics may determine baryon correlations.

The charge separations are therefore computed using the fragmentation models, JETSET and HERWIG, which are constrained to agree with the following experimental information:

(i) $\bar{\delta}$, δ_c and δ_b; for κ = 0.3, 0.5, 1.0, 2.0 and ∞;
(ii) inclusive distributions (from [23]):
  – sphericity, aplanarity,
  – the inclusive charged particle momentum distribution, dN/dz, where z is the fraction of the beam momentum carried by the charged particles,
  – p_T^{in}, the charged particle momentum component transverse to the sphericity axis and projected into the event plane,
  – p_T^{out}, the charged particle momentum component perpendicular to the event plane defined by the sphericity tensor;
(iii) inclusive particle spectra and correlations: K^0, Λ, $\bar{\Lambda}$ from [31];
(iv) $K^\pm$, proton and antiproton spectra from [32];
(v) average multiplicity of $K^{*\pm}$ from [33], K^{*0} from [34].

Systematic errors on charge separations are determined for each model by the quality of the fit to the above mentioned distributions. In practice this is implemented in two different ways. First the experimental errors are artificially increased until a good fit is obtained; this procedure results in an increase of the model parameter errors, and in a corresponding increase in the error on charge separations. Next, poorly reproduced distributions are removed from the fit and the variation of the results is taken as a systematic uncertainty.

For each of the two models considered, a central value and systematic errors are calculated. The consistency of the results validate the procedure. Two important cross-checks

Table 6. Association of JETSET parameters and distributions which constrain their values

u/d – **Symmetric parameters**		
Description	JETSET parameters	Associated distributions
Parton shower parameters	$\Lambda_{\rm QCD}$, $M_{\rm min}$, $\sigma_{\rm pt}$	p_T^{in}, p_T^{out}, S, A, dN/dz
The Lund symmetric fragmentation function	a, b	$\overline{\delta}$, S, A, dN/dz
Resonance production:		
– vector (V) to pseudoscalar (PS) ratio	$V_{ud} \equiv V/(V + PS)_{ud}$	$\langle N(\rho)\rangle$
– tensor meson rate	PARJ(17) PARJ(14)=PARJ(17) × 3/5 PARJ(16)=PARJ(14) PARJ(15)=PARJ(17)× 1/5	$\langle N(f_2)\rangle$
Final state particle dynamics	Bose-Einstein R and Λ η' suppressions	K^0 and π^0 correlations $\langle N\left(\eta'\right)\rangle$
Kaon production		
Description	JETSET parameters	Associated distributions
Rate of production	s/u (= γ_s)	K^0 and $K^{\pm}$ spectra
Resonance production: vector to pseudoscalar ratio	$V_s \equiv V/(V + PS)_s$	$\langle N\left(K^{*0}\right)\rangle$ and $\langle N\left(K^{*\pm}\right)\rangle$
Baryon production		
Description	JETSET parameters	Associated distributions
Rate of production (baryon fraction)	QQ/Q	Proton, Λ spectra
Possible extra degrees of freedom		
– the ratio of strange diquark to non-strange diquark production	(su/du)	Λ spectrum $\langle N\left(\Lambda\overline{\Lambda}\right)\rangle$ pairs
– correlation	popcorn	$\Lambda - \overline{\Lambda}$ correlations
Fix for deficiency		
– baryon suppression	FB Suppr.	High momentum portion of proton and Λ spectra

are performed: the value of $\sin^2\theta_w^{\rm eff}$ extracted from the fit should be independent of the choice of κ, and, given the difficulty in modelling baryon production, the charge of the hemisphere opposite to a fast Λ in hadronic event should be successfully reproduced. Corrections for purely experimental effects are evaluated using the full detector simulation based on JETSET 7.3 as described in Sect. 2. The fits performed to extract the light quark charge separations using JETSET are described in the next section and use JETSET 7.4. The fits performed using HERWIG are described in Sect. 4.5 and use HERWIG 5.6.

4.3 Determination of light quark separations using JETSET

The JETSET model offers a large number of parameters which correspond to uncertainties in the modeling of a variety of physics processes during hadronisation. Light quark jet charge separations are obtained by fitting the JETSET model to the measurements outlined in items (i) to (v) above. The input measurements and distributions are associated with the corresponding parameters of the JETSET model as outlined in Table 6.

The details of the fitting procedure are described in Appendix B. For item (i) in the list of measurements given above, the χ^2 is formed taking into account the correlations between the measurements for different values of κ. Additional correlations between the b and c quark charges are accounted for as described in Sect. 3.3. The method of fitting the inclusive particle spectra to the data is similar to that described in [23]. Improvement of the fitting procedure is obtained by making the approximation that the derivative of cross-sections upon variation of each parameter is independent of the value of the other parameters. This allows a large number of parameters to be varied simultaneously with a manageable number of Monte Carlo samples. The bin-by-bin dependencies of the cross-sections on each of the parameters are computed using JETSET at four values of that model parameter and determining its linear and quadratic dependencies. Each parameter is varied individually, and all other parameters are fixed to their reference values obtained from [23]. The outcome of the procedure is cross-checked by running JETSET with parameters set to the optimum values obtained. The results are shown in Table 7.

In the fit to the proton and Λ spectra two effects are important. Firstly, it is necessary to use the popcorn mechanism as illustrated in Fig. 5. Secondly, in order to reproduce the observed momentum spectra, it is necessary to suppress the production of high momentum baryons. This can be done in

Table 7. Components of the charge separations for κ = 1 according to a JETSET fit to data distributions. Detector effects are included for these values

Separation	Value	Components		
		$\pi^{\pm}$	$K^{\pm}$	$p, \bar{p}$
δ_u	+0.4062	+0.2765	+0.0744	+0.0496
δ_d	−0.2294	−0.2660	+0.0232	+0.0176
δ_s	−0.3287	−0.0451	−0.2929	+0.0188

Table 8. Contributions of the various components of the JETSET fit to the χ^2. W is the deweighting factor used in the fit

Component	W	χ^2	bins
sphericity	12	1.5	22
aplanarity	34	2.0	15
dN/dz	45	4.1	21
p_T^{out}	590	0.8	22
p_T^{in}	140	1.0	28
K^0	1	16.9	28
$K^{\pm}$	1	20.7	29
Λ	1	12.2	21
Proton	1	20.2	24
$\langle N\left(K^{*\pm}\right)\rangle$	1	0.0	1
$\langle N\left(K^{*0}\right)\rangle$	1	0.0	1
$\bar{\delta}$	1	1.2	4
δ_b and δ_c	1	2.3	8

a rather *ad hoc* way in JETSET by tuning the fast baryon suppression parameter.

It is found that a fit to the p_T^{in} and p_T^{out} distributions yields a poor χ^2. This is expected as the parton shower model used does not properly treat the gluon radiation which is responsible for producing the transverse momentum distribution. In order to examine the systematic uncertainty due to this model deficiency the errors on the bins of the p_T^{in} and p_T^{out} distributions are scaled until the prediction and the model agree. In this way the model parameters associated with describing the transverse momentum physics will have errors that reflect the systematic disagreement visible because of the precision of the data. The errors in the data distributions were increased such that each bin in the Monte Carlo distribution was within one sigma (combined statistical and systematic error) of the data value for that bin. More specifically, a single deweighting factor W is defined for the entire distribution such that $\chi_i^2 \rightarrow \left(\chi_i^2/W\right) \leq 1$ for each bin i in the distribution.

The fit to the sphericity and aplanarity distributions also yields a poor χ^2. These distributions contain information about both the fragmentation function and generation of transverse momentum. Since δ constrains the u/d symmetric parameters, including the fragmentation function parameters, the sphericity and aplanarity distributions are not necessary to perform this function and are treated in the same manner as the p_T^{in} and p_T^{out} distributions. Although the dN/dz distribution has a good χ^2, the information obtained about the fragmentation function is also redundant; therefore, this distribution is deweighted in the fit.

Once these deweighting procedures are carried out, the remaining terms in the χ^2 and, in particular, the contribution from $\bar{\delta}$ is about one per degree of freedom. The association of distributions or moments of distributions to specific parameters is an important feature. For example, if the fit is performed without any strange particle information (no kaon or Λ spectra) the error on the rate of strangeness production (s/u) is a factor of 3 larger. This indicates that the parameter is strongly associated to the physics it should describe. As a counter-example, when one attempts to perform a fit with the tensor production parameter free, the model uses this to repair deficiencies in the p_T^{in} and p_T^{out} distributions. The number of f_2's produced is not properly described. It is only when the deweighting is applied to the p_T^{in} and p_T^{out} distributions that a reasonable f_2 rate is predicted. If parameters are found to be affected in this way, they are held fixed during the fit.

Table 9. JETSET parameter values for fits to distributions relevant to charge propagation. The first error is the fit error and the second the systematic uncertainty. Parameters with an "F" beside them were fixed to the values indicated and thus have no fit error

Parameter			Value		
Λ_{QCD}	0.274	±	0.019	±	0.020
M_{min}	0.608	±	0.134	±	0.151
σ_{pt}	0.381	±	0.016	±	0.017
a	0.210	±	0.089	±	0.162
b	0.811	±	0.062	±	0.032
V_{ud}	0.603	±	0.070	±	0.165
Tensor	0.160		F		
V_s	0.466	±	0.036	±	0.048
s/u	0.290	±	0.009	±	0.020
QQ/Q	0.112	±	0.004	±	0.014
su/du	0.723	±	0.062	±	0.121
Popcorn	0.500		F		
Fast Baryon Supr.	0.438	±	0.048	±	0.25
η' Suppression	0.40		F		
Bose-Einstein Λ	1.0		F		
Bose-Einstein R	0.2		F		

The stability of the fit is checked by fixing all the parameters to their best fitted values. Then the distributions are refit one at a time and, simultaneously, the corresponding parameters outlined in Table 6 are allowed to vary. The resulting fit parameters are compared and it is found that the range of values lies within 1σ of the fit errors except for the parameters QQ/Q and b, which lie within 2σ.

The resulting comparison of $\bar{\delta}$ in the data to the Monte Carlo is shown as a function of κ in Fig. 6. The contributions of the various components of the fit to the χ^2 are shown in Table 8.

The fit yields a χ^2 of 73 for 116 degrees of freedom for the distributions which do not have inflated errors. Distributions in ξ, where $\xi = -\log\left(p/E_{beam}\right)$ and p is the particle momentum, are shown in Figs. 7 through 10. The resulting JETSET fit indicated by the solid histograms is compared to the data. The values of the eleven fit parameters and their errors are given in Table 9, including an estimate of the systematic error. The systematic uncertainties are the quadratic sum of the differences induced by removing data distributions and refitting. These systematic studies are described in the following section.

4.4 Systematic uncertainties in the fitted separations

The systematic uncertainties in the charge separation determinations are given in Table 10 and are evaluated as follows:

Table 10. Uncertainties in the separations as determined by JETSET

Systematic error	Item changed	$\Delta\delta_u$	$\Delta\delta_d$	$\Delta\delta_s$
p_T description	Remove $p_T^{in/out}$, S, A, dN/dz	± 0.0010	± 0.0017	± 0.0007
Higher spin state contribution	PARJ(17)= 0.16 ± 0.1	± 0.0040	± 0.0020	± 0.0011
b,c contamination in spectrum	$K^0/K^\pm$ discrepancy	± 0.0047	± 0.0016	± 0.0025
Baryon model failures	Popcorn = 0.50 ± 0.18	± 0.0051	± 0.0044	± 0.0036
Baryon model failures	FB supr. = 0.50 ± 0.25	± 0.0002	± 0.0069	± 0.0011
Total systematic error		± 0.0081	± 0.0087	± 0.0047
Fit uncertainty		± 0.0026	± 0.0045	± 0.0017
Total uncertainty		± 0.0085	± 0.0098	± 0.0050

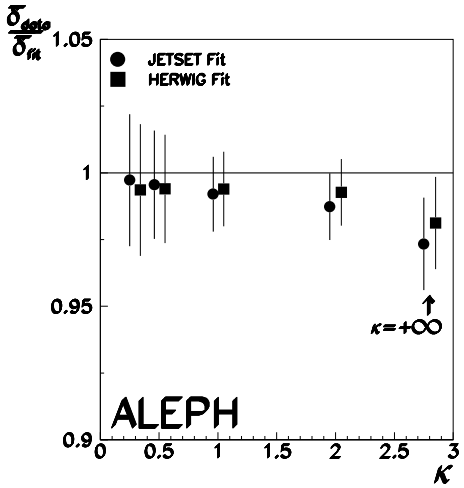

Fig. 6. The ratio of $\bar{\delta}$ in the data to that fitted from the Monte Carlo, plotted as a function of κ for JETSET and HERWIG fits. Error bars represent the statistical and systematic uncertainties in data and the statistical error on the Monte Carlo

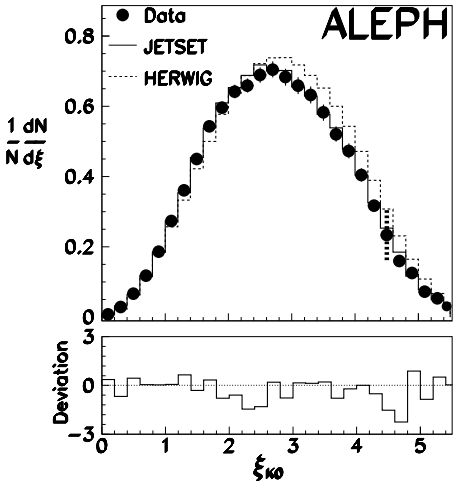

Fig. 7. Neutral kaon spectrum compared to the JETSET (solid) and HERWIG (dashed) Monte Carlos. The spectrum is described in terms of the momentum fraction of the beam energy that the neutral kaon carries by $\xi = -\log\left(p/E_{\rm beam}\right)$. The dashed error bar gives one example of the deweighting factor of 30 in the χ^2 used for the HERWIG fit. No deweighting is used for JETSET. The number of standard deviations of the JETSET prediction from the data is shown by the solid line in the lower portion of the figure and includes statistical and systematic errors added in quadrature

– *Transverse momentum description.* As noted previously, the transverse momentum is not well described by JETSET. The distributions of p_T^{in}, p_T^{out}, S, A, and dN/dz are removed from the fit and the systematic error estimate from this weakness in the model is taken as half the change in the separations.

– *Tensor meson production.* Current measurements of tensor meson production remain rather uncertain. In addition, the same parameter is used in kaon and pion production. This mixes u/d asymmetric and symmetric components. Adding $\langle N(f_2)\rangle$ [33] to the quantities fitted for JETSET and simultaneously releasing the tensor meson production parameters gives a value of PARJ(17)= 0.13 ± 0.03 and the remainder of the fit does not change. The error has been tripled relative to the fitted value obtained by including the number of f_2's observed by taking PARJ(17)= 0.16 ± 0.1.

– *Charged and neutral kaon discrepancy.* The fitted value of the parameter describing the rate of kaons depends on whether the charged or neutral kaon spectrum is used in the fit. Heavy flavour decays to charged and neutral kaons are a background to the production of kaons during fragmentation of light quarks. The agreement of the Monte Carlo prediction of the heavy flavour jet charges with data indicates that the kaon contributions are modelled well in JETSET 7.4. Furthermore kaon decays from the heavy flavours are concentrated in the region $1.5 \leq \xi \leq 3.0$ and in this region the kaon spectra fit well. The heavy flavour decay rates to charged kaons are expected to be different from the decay rates to neutral kaons; hence, an estimate of the residual error due to this background is taken to be half the difference in the value of the jet charge separations obtained when fitting one or the other kaon spectrum.

– *Popcorn mechanism.* The popcorn mechanism is an approximate description of a baryon production mechanism which allows for new dynamics beyond those prescribed by the fragmentation function. It affects both the correlation between baryon pairs and the transverse momentum spectra; therefore, systematic uncertainties in the spectra will be fed artificially into this parameter during the fit, resulting in baryon production being used to repair deficiencies in the perturbative QCD description. The parameter has been fixed to the value obtained in an earlier publication [31] on Λ–$\bar{\Lambda}$ correlations. The systematic error attributed to possible new dynamics affecting baryon correlations is obtained by repeating the fit at popcorn values of 0.32 and 0.68. If the popcorn parameter is allowed to vary and the Λ–$\bar{\Lambda}$ correlation data are included, a value of 0.39 ± 0.18 is obtained.

– *Fast baryon suppression.* The model for baryon production fails to reproduce the data at high momentum. A parameter which artificially suppresses baryons produced from a first-rank quark can be adjusted to give an excellent fit to both the proton and Λ spectra. However, given the *ad hoc* nature of this parameter, and the possibility of dynamic differences that could arise in a proper description of the true mechanism for baryon suppression at high momenta, a rather large range of values is taken. It is remarkable that the u quark charge does not change when the baryon supression parameter is varied while the d quark charge is affected. First rank baryon production contributes a positive charge to the u quark charge separation and a negative charge to the d quark charge separation. Second rank baryon production contributes a positive charge to both quark charge separations. The proton data require increased production of second rank baryons to replace the supressed first rank baryons. Thus the second rank baryons compensate the u quark charge loss from first rank whereas in the d quark case opposite signs in first and second rank baryon production prevent compensation. As shown in Fig. 11, checks of the baryon production mechanism using fast Λ's to tag s quarks indicate that the jet charge in the opposite hemisphere is properly reproduced if one uses a baryon suppression in the range chosen.
– *Final state interactions.* The impact on the fit when varying the η' suppression and Bose-Einstein parameters is found to be negligible. In addition, including $\langle N\left(\eta'\right)\rangle = 0.068 \pm 0.018 \pm 0.016$ from [35] in the JETSET fit and simultaneously releasing the η' suppression parameter gives a value of 0.35 ± 0.10 for the η' suppression parameter and the remainder of the fit does not change.
– *Fit procedure.* The fit to Monte Carlo involves linear excursions in parameter space around a central reference point. Finite statistics in determining the linear parameterization around the reference point are included as a systematic error. An upper limit on the effects of systematic differences between Monte Carlo versions is evaluated by taking half the change obtained when fitting with JETSET 7.3 and 7.4. Finally, as mentioned above, the

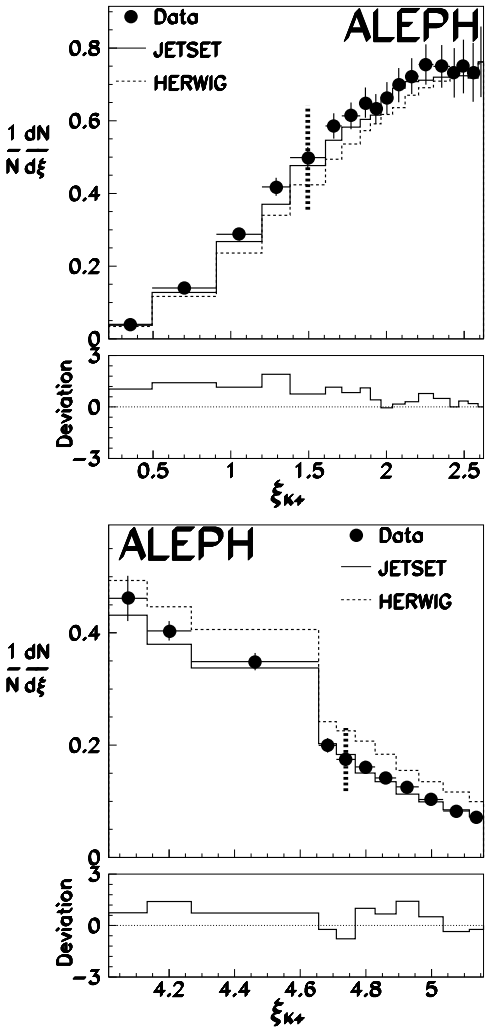

Fig. 8. As for the previous figure but for the charged kaon spectrum. A deweighting factor of 24 is used for HERWIG in this case

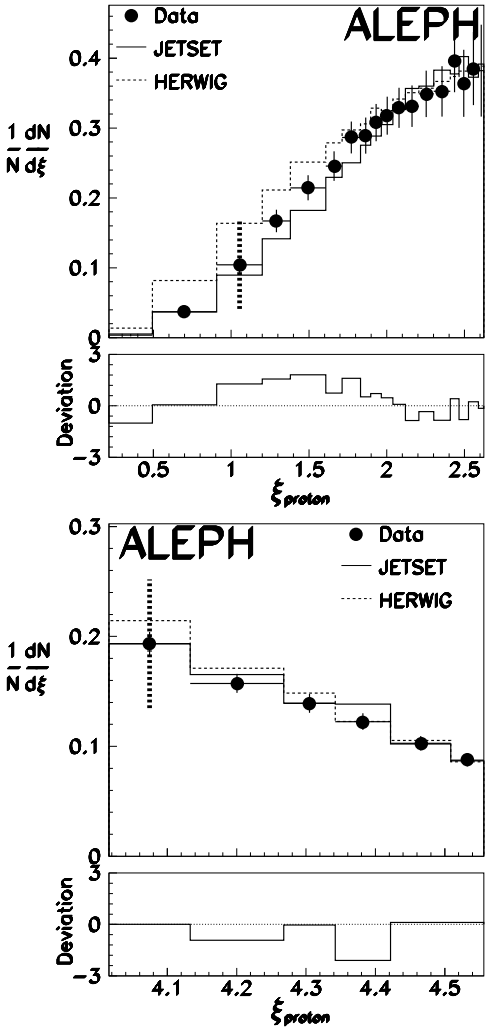

Fig. 9. As for the previous figure but for the proton spectrum. A deweighting factor of 30 is used for HERWIG in this case

dN/dz distribution contains the same information about the fragmentation function as δ. Thus, the deweighting is removed as a systematic check.

The statistical and systematic errors on the fitted distributions are added in quadrature with these systematic errors to yield the total error in the light quark charge separations.

4.5 Determination of light quark charge separations using HERWIG

The HERWIG hadronisation model is used to extract the light quark charge separations using a similar fit procedure to that described previously. The philosophy of the model differs from that of JETSET so the fit procedure is modified accordingly. For HERWIG only three tunable parameters are used [1]. One of these, $M_{cluster}$, is strongly determined by δ which does not constrain the other two at all. Fitting to δ and the kaon spectrum gives constraints on all three parameters whereas fitting δ and the Λ or proton spectrum also constrains the parameters but to different values. The model is unable to reproduce all spectra simultaneously. In addition, HERWIG is unable to reproduce observed correlations between baryons [31], indicating that the true discrepancy lies in the treatment of baryon production. As a consequence, the range of values which reproduces each spectrum separately is used to estimate the systematic uncertainty on the charge separations.

The various contributions of the χ^2 are detailed in Table 11. The fit is dominated by systematic discrepancies of the model with the data and hence a statistical interpretation of the fit quality is not possible. The distributions in Figs. 7 through 10 show the resulting HERWIG fit compared to the data. In each case an example of the deweighted error bar is also shown. The final fitted values of the model parameters are given in Table 12 with the systematic error contributions given in Table 13.

The results for the charge separations are given in Table 14. As shown in Fig. 6, both HERWIG and JETSET reproduce the basic charge transfer process of the symmetric components with a high degree of accuracy over the full range of κ values. The separations determined with HERWIG are consistent within the systematic errors with those quoted for JETSET. However, it is clear from the deweighting necessary in HERWIG for the key spectra that it is not well-suited for describing charge propagation for the u/d-symmetry-breaking components.

[1] It has been pointed out by the authors of HERWIG that more tunable parameters could now be used

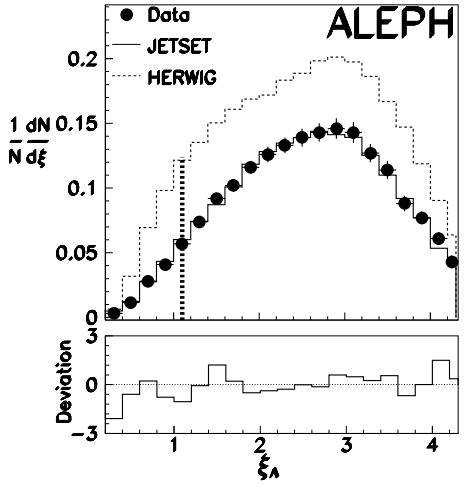

Fig. 10. As for the previous figure but for the Λ spectrum. A deweighting factor of 500 is used for HERWIG in this case

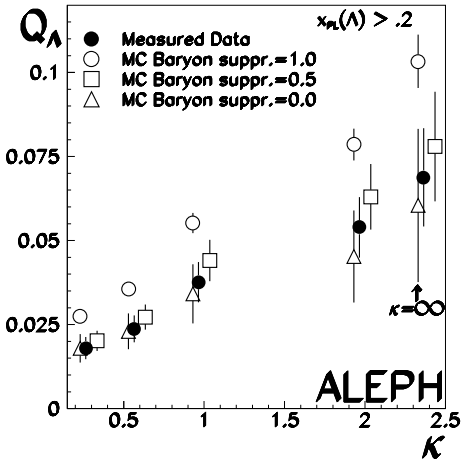

Fig. 11. Comparison of the charge opposite a Λ to the JETSET prediction plotted as a function of κ and for $x_\Lambda = p_\Lambda/E_{\rm beam} > 0.2$. The JETSET Monte Carlo is compared to the data for various settings of the fast baryon suppression parameter

Table 11. Contributions to the χ^2 of the various components of the HERWIG fit. W is the deweighting factor used in the fit

Component	W	χ^2	Bins
Sphericity	12	5.8	22
Aplanarity	34	3.8	15
dN/dz	45	9.5	21
p_T^{out}	5	10.6	22
p_T^{in}	5	14.5	28
K^0	30	7.7	28
$K^\pm$	24	8.7	29
Λ	500	5.7	21
Proton	30	5.1	24
$\langle N\left(K^{*\pm}\right)\rangle$	1	0.5	1
$\langle N\left(K^{*0}\right)\rangle$	1	0.0	1
$\bar{\delta}$	1	0.8	4
δ_b and δ_c	1	1.8	8

5 Determination of $\sin^2\theta_w^{\rm eff}$

The value of $\sin^2\theta_w^{\rm eff}$ predicted by the ALEPH data in this analysis is determined within the context of the Standard Model using (3). The acceptance factor, $A_{\rm acc}$, is calculated using (4) and cross-checked using Monte Carlo simulation

Table 12. HERWIG parameter values for fits to distributions relevant to charge propagation

Parameter			Value		
Λ_{LL}	0.176	$\pm$	0.003	$\pm$	0.140
M_{gluon}	0.728	$\pm$	0.024	$\pm$	0.302
$M_{cluster}$	3.700	$\pm$	0.043	$\pm$	0.428

Table 13. Uncertainties in the separations as determined by HERWIG

Systematic error	Item changed	$\Delta\delta_u$	$\Delta\delta_d$	$\Delta\delta_s$
p_T description	Remove $p_T^{in/out}$, S, A, dN/dz from fit	$\pm$0.0139	$\pm$0.0040	$\pm$0.0061
Baryon/kaon inconsistency	Fit using only $p_T^{in/out}$, S, A, dN/dz	$\pm$0.0016	$\pm$0.0046	$\pm$0.0046
b,c contamination	$K^0/K^\pm$ discrepancy	$\pm$0.0001	$\pm$0.0004	$\pm$0.0004
Baryon model inconsistency	Exclude Λ/p spectra	$\pm$0.0012	$\pm$0.0032	$\pm$0.0034
Baryon model inconsistency	Fit only Λ/p spectra, $\bar{\delta}$	$\pm$0.0281	$\pm$0.0085	$\pm$0.0130
Baryon model inconsistency	Exclude the $K^0/K^\pm$ spectra	$\pm$0.0002	$\pm$0.0005	$\pm$0.0006
Baryon model inconsistency	Fit only $K^0/K^\pm$ spectra, $\bar{\delta}$	$\pm$0.0008	$\pm$0.0045	$\pm$0.0044
Total systematic uncertainty		$\pm$0.0314	$\pm$0.0118	$\pm$0.0161
Fit uncertainty		$\pm$0.0021	$\pm$0.0052	$\pm$0.0054
Total uncertainty		$\pm$0.0315	$\pm$0.0129	$\pm$0.0170

to take into account the efficiency of the hadronic event selection and any dependence on quark flavour. These are found to result in a small shift of the extracted $\sin^2\theta_w^{\rm eff}$ by 0.00006 and are neglected. The value of $\sin^2\theta_w^{\rm eff}$ is varied in ZFITTER [14] to obtain A_{FB}^f and Γ_f in (3). This, together with the measured charge separations and inclusive particle distributions, gives a prediction of the forward-backward charge asymmetry that is fitted to the measured values of $\langle Q_{FB}\rangle$ in Table 1. The energy dependence of asymmetries being approximately linear, data are binned into the three energy points shown in Table 15.

QCD effects [36] are potentially of two kinds: spin flip by gluon emission or vertex diagrams and angular kick to the final state quarks due to final state gluon radiation. This first effect is suppressed by $(m_q/m_Z)^2$ terms, is extremely small ($\mathcal{O}\left(10^{-3}\right)$ of the asymmetry itself) and is thus neglected. The effect of the angular kick leads to a $(1-\alpha_s/\pi)$ correction, which is 4% of the asymmetry. However, in the determination of δ and in the calculation of jet charges from Monte Carlo, this gluon smearing is already taken into account by defining the charge separations relative to the quark direction prior to gluon radiation. The only remaining uncertainty concerns the accuracy of JETSET in describing first and second order gluon emission and b quark mass effects. The first order is explicitly implemented in JETSET, but the second order is uncertain. This error is evaluated as the full size of the second order effect plus the uncertainty in the first order arising from the error on α_s: this is at most 0.5% of the asymmetry which is $\Delta\sin^2\theta_w^{\rm eff} = 0.00009$. The b mass effect is 20% of the QCD correction for that quark. Taking this as the error yields $\Delta\sin^2\theta_w^{\rm eff} = 0.0002$ on the b quark asymmetry. For the inclusive asymmetry the effect is reduced to $\Delta\sin^2\theta_w^{\rm eff} = 0.0001$ because of cancellations between quark flavours. Adding the two errors yields $\Delta\sin^2\theta_w^{\rm eff} = 0.00017$. Since QCD corrections to the asymmetries are incorporated into the definition of jet charges, they are explicitly deactivated in ZFITTER during the fit. However, QCD contributions to the partial widths are included.

The fit is performed for measurements of $\langle Q_{FB}\rangle$ for the three energies shown in Table 15 and κ = 0.3, 0.5, 1.0, 2.0 and ∞ with the correlations between the different values of κ taken into account for both the charge separations and $\langle Q_{FB}\rangle$. Details of the fit are described in Appendix B.2. To check for hadronisation model dependence, charge separations are obtained both with HERWIG and JETSET. The results are

$$\sin^2\theta_w^{\rm eff} = 0.23222 \pm 0.00081(\text{exp. stat.}) \pm 0.00070(\text{exp. syst.}) \pm 0.00080(\text{sep.}). \quad (\text{JETSET}) \quad (23)$$

with a χ^2 of 88 for 128 degrees of freedom, and

$$\sin^2\theta_w^{\rm eff} = 0.23324 \pm 0.00081(\text{exp. stat.}) \pm 0.00070(\text{exp. syst.}) \pm 0.00161(\text{sep.}) \quad (\text{HERWIG}) \quad (24)$$

with a χ^2 of 8 for 12 degrees of freedom. In the case in which HERWIG separations are used, only the $\langle Q_{FB}\rangle$ measurements are used to calculate the χ^2/DOF because the fit of the model to data is systematically limited. These results are independent of κ as shown in Fig. 12, where $\sin^2\theta_w^{\rm eff}$ is plotted as a function of κ; the statistical correlations amongst κ values have been taken into account. The effect of these is indicated by "uncorrelated error" in the figure. A description of how the correlations are handled is in Appendix B.3. The results using the two models in determining the light quark charge separations are consistent within their systematic errors. The JETSET result is more precise and is taken as the final value. Systematic uncertainties on the charge separations are propagated through to the measurement of $\sin^2\theta_w^{\rm eff}$ as shown in Table 16 for JETSET and in Table 17 for HERWIG.

Table 14. Components of the charge separations for κ = 1 according to a HERWIG fit to data distributions. Detector effects are included for these values

Separation	Value	Components		
		$\pi^\pm$	$K^\pm$	$p,\bar{p}$
δ_u	+0.3988	+0.2935	+0.0689	+0.0263
δ_d	$-$0.2473	$-$0.2673	+0.0322	$-$0.0048
δ_s	$-$0.3294	$-$0.0447	$-$0.2503	$-$0.0030

Systematic uncertainties that are independent of the hadronisation model are detailed in Table 18. The statistical errors from the parameter fits are shown and include the errors on the b and c quark separations as well as that on δ. The dependency of $\langle Q_{FB}\rangle$ on centre-of-mass energy is shown for κ = 1.0 in Fig. 13 and compared to the expectation using the fitted value of $\sin^2\theta_w^{\rm eff}$ and the JETSET separations. The three curves reflect the uncertainty in the charge separations.

The value of $\sin^2\theta_w^{\rm eff}$ determined here is statistically correlated with the published value from the ALEPH $A_{FB}^{b\bar{b}}$ analysis [6] based upon lifetime tagging. The correlation is estimated from the overlap in event samples to be 29%. In addition the systematic uncertainty from $\Delta\delta_b$ and QCD effects in Table 18 is fully correlated with an uncertainty

Table 15. Hadronic Z decays and their asymmetries for various κ values as recorded by the ALEPH detector between 1990 and 1994 around the Z peak

$\langle\sqrt{s}\rangle$ (GeV)	$Z \to q\bar{q}$	$\langle Q_{FB}\rangle \times 10^4$				
		$\kappa = 0.3$	$\kappa = 0.5$	$\kappa = 1.0$	$\kappa = 2.0$	$\kappa = \infty$
89.52	104396	-63.8 ± 10.8	-76.7 ± 12.6	-103.4 ± 18.8	-126.1 ± 28.1	-114.4 ± 44.8
91.25	2215519	-43.1 ± 2.3	-56.8 ± 2.7	-88.6 ± 4.1	-125.5 ± 6.1	-147.0 ± 9.7
92.93	158545	-40.9 ± 8.6	-56.0 ± 10.1	-92.8 ± 15.2	-135.6 ± 22.7	-151.3 ± 36.4

Table 16. Systematic errors on $\sin^2\theta_w^{eff}$ due to uncertainties in the determination of the charge separations computed from JETSET

Systematic error	Item changed	$\Delta\sin^2\theta_w^{eff}$
p_T description	Remove $p_T^{in/out}$, S, A, dN/dz from fit	± 0.00010
Higher spin state contribution	P(17)= 0.16 ± 0.1	± 0.00018
b,c contamination in spectrum	$K^0/K^{\pm}$ discrepancy	± 0.00020
Baryon model failures	Popcorn = 0.5 ± 0.18	± 0.00048
Baryon model failures	FB Supr. = 0.5 ± 0.25	± 0.00024
Fit procedure	No weight on dN/dz	± 0.00019
Fit procedure	Linearity of fit	± 0.00010
Fit procedure	Consistency of MC versions	± 0.00015
Total		± 0.00066

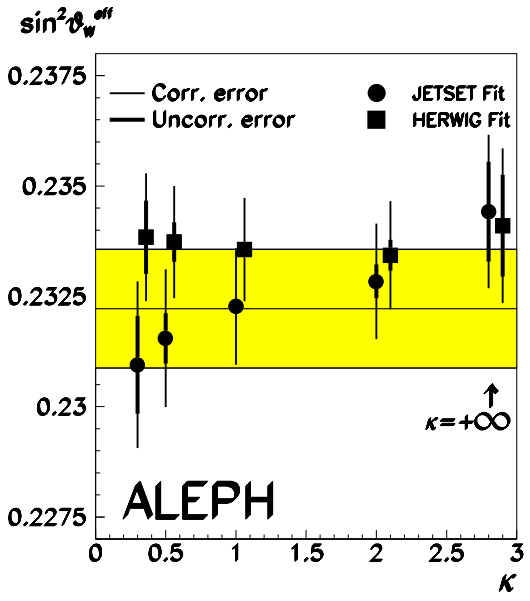

Fig. 12. The value of $\sin^2\theta_w^{eff}$ plotted as a function of κ using separations both from the JETSET and HERWIG Monte Carlos and $\langle Q_{FB}\rangle$ for the Z peak energy. The errors (thick lines) shown are relative to the value obtained at $\kappa = 1.0$. The errors for each point are indicated by the extensions (thin lines) of the errors. The shaded region represents the final result with its total error. The systematic errors given in Tables 16 and 17 are not included in the points in the figure. Since they are not fully correlated as a function of κ, they could be responsible for some of the variations of $\sin^2\theta_w^{eff}$ with κ

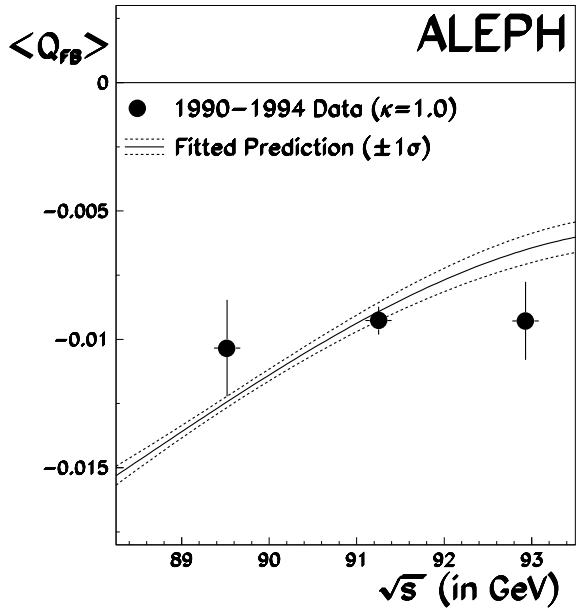

Fig. 13. $\langle Q_{FB}\rangle$ plotted as a function of centre-of-mass energy for the data (points) and a prediction using the fitted values of the JETSET light quark charge separations, the measured values of the heavy quark charge separations and the fitted value of $\sin^2\theta_w^{eff}$. The family of curves reflects the errors on the quark charge separations. The results are shown for $\kappa = 1.0$

$\Delta\sin^2\theta_w^{eff} = 0.00066$ from the measurement of δ_b in the $A_{FB}^{b\bar{b}}$ analysis.

6 Summary and conclusions

A value of $\sin^2\theta_w^{eff}$ has been determined within the context of the Standard Model from a measurement of the forward-backward charge asymmetry of hadronic events

$$\sin^2\theta_w^{eff} = 0.2322 \pm 0.0008(\text{exp. stat.}) \pm 0.0007(\text{exp. syst.}) \pm 0.0008(\text{sep.}). \quad (25)$$

This corresponds to a top quark mass of $m_{top} = 170 \pm 42$ GeV/c^2 for $m_{Higgs} = 300$ GeV/c^2. Jet charges have been measured in hadronic Z decays for b and c quarks directly and for light quark flavours using hadronisation models constrained through the measurement of δ and inclusive particle distributions. The results for $\kappa = 1.0$ are summarized in Table 19. For heavy flavours, the jet charge separations were extracted by studying the dependence of the average charge separation δ on the b, c and uds quark purities in the event sample as controlled by the lifetime tag method. In the case of the charm quark, a second method using D^* tagging was also employed and found to be in agreement with the lifetime-tag method. The two methods were combined to give the best precision on the measurements of the jet charge separations.

Table 17. Systematic errors on $\sin^2\theta_w^{\rm eff}$ due to uncertainties in the determination of the charge separations computed from HERWIG

Systematic error	Item changed	$\Delta\sin^2\theta_w^{\rm eff}$
p_T description	Remove $p_T^{in/out}$, S, A, dN/dz from fit	±0.00075
Baryon/strangeness inconsistency	Fit using only $p_T^{in/out}$	±0.00046
b,c contamination in spectrum	$K^0/K^\pm$ discrepancy	±0.00003
Baryon model inconsistency	Exclude Λ/p spectra	±0.00034
Baryon model inconsistency	Fit only Λ/p spectra, $\bar{\delta}$	±0.00116
Baryon model inconsistency	Exclude the $K^0/K^\pm$ spectra	±0.00005
Baryon model inconsistency	Fit only the $K^0/K^\pm$ spectra, $\bar{\delta}$	±0.00044
Total		±0.00156

Table 18. Computation of systematic errors on $\sin^2\theta_w^{\rm eff}$ due to uncertainties in the determination of the charge separations and which are independent of the hadronisation model used in determination of the light quark separations

Systematic error	$\Delta\sin^2\theta_w^{\rm eff}$
$\Delta\delta_c$	±0.00033
$\Delta\delta_b$	±0.00024
$\Delta\delta$	±0.00005
Statistical and systematic errors from distributions	±0.00002
QCD effects	±0.00017
Total	±0.00045

Table 19. The charge separations including detector effects for $\kappa = 1$

Separation	Value	
	JETSET	HERWIG
δ_u	$+0.4062 \pm 0.0081$	$+0.3988 \pm 0.0315$
δ_d	-0.2294 ± 0.0087	-0.2473 ± 0.0129
δ_s	-0.3287 ± 0.0047	-0.3294 ± 0.0170

Separation	Value
δ_c	$+0.1996 \pm 0.0174$
δ_b	-0.2057 ± 0.0061

It was shown that the differences between light quark charge separations arise from the breaking of u/d-symmetry due to the production of strange particles and baryons during hadronisation. The average jet charge separation $\bar{\delta}$ however, is sensitive to the u/d symmetric component and relatively insensitive to the asymmetric contributions. The JETSET and HERWIG hadronisation models reproduce the symmetric jet charge component to an accuracy of 2%. From particle multiplicity measurements in kaons, protons and Λ's, it is known that both symmetry-breaking processes occur with a mean frequency of once per event. The basic charge propagation described by the hadronisation models were therefore fitted to single particle inclusive spectra and correlations of kaons, protons and Λ's to obtain the jet charge contributions from the symmetry-breaking components. It was found that the JETSET model was able to reproduce these spectra although it was also necessary to use rather *ad hoc* parameters (e.g. fast baryon suppression) in the baryon modeling. The HERWIG model was unable to simultaneously reproduce the basic jet charge together with the baryon and kaon spectra.

The jet charge separations for light quarks were extracted from the hadronisation models together with independent systematic errors for each model. These separations agree in both hadronisation models although the systematic error is significantly smaller for those determined using JETSET than HERWIG. The systematic errors were propagated through to the determination of $\sin^2\theta_w^{\rm eff}$. The two models gave consistent answers. The more precise result was obtained using JETSET charge separations.

Table 20. $\bar{\delta}$ correlations amongst κ values

	$\kappa = 0.3$	$\kappa = 0.5$	$\kappa = 1.0$	$\kappa = 2.0$	$\kappa = \infty$
$\kappa = 0.3$	1.000	0.936	0.663	0.423	0.206
$\kappa = 0.5$		1.000	0.865	0.635	0.336
$\kappa = 1.0$			1.000	0.909	0.553
$\kappa = 2.0$				1.000	0.731
$\kappa = \infty$					1.000

Acknowledgements. We wish to thank our colleagues from the accelerator divisions for the successful operation of the LEP machine, and the engineers and technical staff in all our institutions for their contribution to the good performance of ALEPH. Those of us from non-member states thank CERN for its hospitality.

Appendix A: material effects on asymmetry measurements

For quarks (antiquarks) of flavour f ($\bar{\rm f}$) in hemisphere H (= F,B) the detector effects, $\varepsilon_{\rm f}^{\rm H}$ ($\varepsilon_{\bar{\rm f}}^{\rm H}$) are defined as

$$\langle Q_{\rm f}^{\rm det}\rangle^{\rm H} = \langle Q_{\rm f}^{\rm gen}\rangle + \varepsilon_{\rm f}^{\rm H} \tag{26}$$

$$\langle Q_{\bar{\rm f}}^{\rm det}\rangle^{\rm H} = \langle Q_{\bar{\rm f}}^{\rm gen}\rangle + \varepsilon_{\bar{\rm f}}^{\rm H} = -\langle Q_{\rm f}^{\rm gen}\rangle + \varepsilon_{\bar{\rm f}}^{\rm H}, \tag{27}$$

where $\langle Q_{\rm f}^{\rm det}\rangle^{\rm H}$ is the average hemisphere charge including detector effects. The jet charge in either the forward or backward hemisphere in the absence of a detector is $\langle Q_{\rm f}^{\rm gen}\rangle$. A material asymmetry for secondary interactions is written as

$$A_{\rm mat} = \frac{\varepsilon_{\rm f}^{\rm F} - \varepsilon_{\rm f}^{\rm B}}{\varepsilon_{\rm f}^{\rm F} + \varepsilon_{\rm f}^{\rm B}} = \frac{\varepsilon_{\rm f}^{\rm F} - \varepsilon_{\rm f}^{\rm B}}{2\varepsilon_{\rm f}} \tag{28}$$

where the average detector effect for quark f is $\varepsilon_{\rm f} \equiv \left(\varepsilon_{\rm f}^{\rm F} + \varepsilon_{\rm f}^{\rm B}\right)/2$. A similar equation for the antiquark defines $A_{\rm mat}$

$$\bar{A}_{\rm mat} = \frac{\varepsilon_{\bar{\rm f}}^{\rm F} - \varepsilon_{\bar{\rm f}}^{\rm B}}{\varepsilon_{\bar{\rm f}}^{\rm F} + \varepsilon_{\bar{\rm f}}^{\rm B}} = \frac{\varepsilon_{\bar{\rm f}}^{\rm F} - \varepsilon_{\bar{\rm f}}^{\rm B}}{2\varepsilon_{\bar{\rm f}}}. \tag{29}$$

The observed average charge of quark f is

$$\langle Q_{\rm f}^{\rm det}\rangle = \frac{\sigma_{\rm f}^{\rm F}}{\sigma_{\rm f}}\langle Q_{\rm f}^{\rm det}\rangle^{\rm F} + \frac{\sigma_{\rm f}^{\rm B}}{\sigma_{\rm f}}\langle Q_{\rm f}^{\rm det}\rangle^{\rm B} \tag{30}$$

where $\sigma_{\rm f}$ is the total rate for $e^+e^- \to {\rm Z}/\gamma \to {\rm f\bar{f}}$ and $\sigma_{\rm f}^{\rm F(B)}$ is the rate for quarks in the forward (backward) hemisphere with

Table 21. Correlation matrix for the combined b and c quark charge separations

	δ_c $\kappa = 0.3$	δ_c $\kappa = 0.5$	δ_c $\kappa = 1.0$	δ_c $\kappa = 2.0$	δ_c $\kappa = \infty$	δ_b $\kappa = 0.3$	δ_b $\kappa = 0.5$	δ_b $\kappa = 1.0$	δ_b $\kappa = 2.0$	δ_b $\kappa = \infty$
δ_c, $\kappa = 0.3$	+1.000	+0.485	+0.373	+0.320	+0.217	−0.731	−0.345	−0.260	−0.224	−0.146
δ_c, $\kappa = 0.5$		+1.000	+0.482	+0.400	+0.287	−0.341	−0.708	−0.338	−0.282	−0.201
δ_c, $\kappa = 1.0$			+1.000	+0.866	+0.635	−0.235	−0.301	−0.634	−0.558	−0.422
δ_c, $\kappa = 2.0$				+1.000	+0.766	−0.161	−0.206	−0.466	−0.558	−0.449
δ_c, $\kappa = \infty$					+1.000	−0.019	−0.042	−0.126	−0.177	−0.265
δ_b, $\kappa = 0.3$						+1.000	+0.426	+0.283	+0.223	+0.058
δ_b, $\kappa = 0.5$							+1.000	+0.423	+0.330	+0.153
δ_b, $\kappa = 1.0$								+1.000	+0.866	+0.578
δ_b, $\kappa = 2.0$									+1.000	+0.736
δ_b, $\kappa = \infty$										+1.000

Table 22. $\langle Q_{FB} \rangle$ correlations amongst κ values

	$\kappa = 0.3$	$\kappa = 0.5$	$\kappa = 1.0$	$\kappa = 2.0$	$\kappa = \infty$
$\kappa = 0.3$	1.000	0.966	0.818	0.669	0.481
$\kappa = 0.5$		1.000	0.935	0.815	0.607
$\kappa = 1.0$			1.000	0.958	0.759
$\kappa = 2.0$				1.000	0.862
$\kappa = \infty$					1.000

$$\sigma_f^F = \frac{1}{2}\sigma_f \left(1 + A_{FB}^f\right) = \sigma_{\bar{f}}^B \tag{31}$$

$$\sigma_f^B = \frac{1}{2}\sigma_f \left(1 - A_{FB}^f\right) = \sigma_{\bar{f}}^F. \tag{32}$$

It follows from the equations above that the detected charges for quark f and antiquark $\bar{f}$ are

$$\langle Q_f^{det} \rangle = \langle Q_f^{gen} \rangle + \varepsilon_f + \varepsilon_f A_{FB}^f A_{mat} \tag{33}$$

$$\langle Q_{\bar{f}}^{det} \rangle = -\langle Q_{\bar{f}}^{gen} \rangle + \varepsilon_{\bar{f}} - \varepsilon_{\bar{f}} A_{FB}^f \bar{A}_{mat}, \tag{34}$$

so that from (2) the detected charge separation for a quark f is

$$\delta_f^{det} = \langle Q_f^{det} - Q_{\bar{f}}^{det} \rangle = \delta_f^{gen} + \varepsilon_f - \varepsilon_{\bar{f}} + A_{FB}^f \left(\varepsilon_f A_{mat} + \varepsilon_{\bar{f}} \bar{A}_{mat}\right) \tag{35}$$

and the total charge from the quark f is

$$\langle Q_f^{det} + Q_{\bar{f}}^{det} \rangle = \varepsilon_f + \varepsilon_{\bar{f}} + A_{FB}^f \left(\varepsilon_f A_{mat} - \varepsilon_{\bar{f}} \bar{A}_{mat}\right). \tag{36}$$

The last terms in (33) to (36) are very small, $\mathcal{O}\left(10^{-5}\right)$, and neglected in the following. With (35) it is possible to rewrite (11) as

$$\left(\bar{\delta}_f^{det}\right)^2 = \left(\delta_f^{gen} + \varepsilon_f - \varepsilon_{\bar{f}}\right)^2 - \left(\langle Q_{FB} \rangle_f^{det}\right)^2 + \langle \mathscr{R}_f^{det} \mathscr{R}_{\bar{f}}^{det} \rangle \tag{37}$$

Thus a measurement of $\bar{\delta}_f^{det}$ includes a possible difference between ε_f and $\varepsilon_{\bar{f}}$.

A similar procedure is used to compute the forward /backward charge asymmetry for a sample of $e^+e^- \rightarrow Z/\gamma \rightarrow f\bar{f}$ events for a single flavour $\langle Q_{FB} \rangle_f = \langle Q_F \rangle_f - \langle Q_B \rangle_f$ where

$$\langle Q_F \rangle_f = \frac{\sigma_f^F}{\sigma_f} \langle Q_f \rangle^F + \frac{\sigma_{\bar{f}}^F}{\sigma_f} \langle Q_{\bar{f}} \rangle^F \tag{38}$$

$$\langle Q_B \rangle_f = \frac{\sigma_f^B}{\sigma_f} \langle Q_f \rangle^B + \frac{\sigma_{\bar{f}}^B}{\sigma_f} \langle Q_{\bar{f}} \rangle^B. \tag{39}$$

It follows that

$$\langle Q_{FB} \rangle_f^{det} = A_{FB}^f \left(\delta_f^{gen} + \varepsilon_f - \varepsilon_{\bar{f}}\right) + \varepsilon_f A_{mat} + \varepsilon_{\bar{f}} \bar{A}_{mat} \tag{40}$$

$$\simeq A_{FB}^f \left(\delta_f^{gen} + \varepsilon_f - \varepsilon_{\bar{f}}\right) + A_{mat} \left(\varepsilon_f + \varepsilon_{\bar{f}}\right) \tag{41}$$

and

$$\langle Q \rangle_f^{det} = \langle Q_F + Q_B \rangle_f^{det} \simeq \varepsilon_f + \varepsilon_{\bar{f}}, \tag{42}$$

where terms in $A_{mat} A_{FB}^f \left(\varepsilon_f - \varepsilon_{\bar{f}}\right)$ are ignored and any difference between A_{mat} and $\bar{A}_{mat}$ is neglected. Thus,

$$\langle Q_{FB} \rangle_f^{det} = A_{FB}^f \delta_f^{det} + A_{mat} \langle Q \rangle_f^{det}. \tag{43}$$

Appendix B: fitting procedures

In this appendix the fitting procedures used to obtain the separations and those used to obtain $\sin^2\theta_w^{eff}$ are described. Details of the test of the κ dependence of $\sin^2\theta_w^{eff}$ are also given.

B.1 Fitting the separations

The fitting procedure used to obtain the separations for both JETSET and HERWIG consists of minimizing

$$\chi^2_{sep} = \chi^2_{QCD} + \chi^2_{\delta} + \chi^2_{heavy}. \tag{44}$$

For QCD there is a Monte Carlo prediction y_{MC}^{ij} for each bin i of each of the measured distribution j. This prediction is described by the central value y_0^{ij} obtained from the reference parameter settings p_0^k for each parameter p^k and a linear slope m^{ijk} describing the dependence of y_{MC}^{ij} on the excursion of each Monte Carlo parameter away from its central value. Thus, the prediction for each bin of each distribution is given by

$$y_{MC}^{ij} = y_0^{ij} + \sum_k m^{ijk} \left(p^k - p_0^k\right) \tag{45}$$

where m^{ijk} is determined by running the Monte Carlo at four settings of each parameter and performing a linear fit to the contents of each bin of each distribution. Finally,

$$\chi^2_{QCD} = \sum_{ij} \frac{\left(\Delta_{QCD}\right)^2_{ij}}{w^j \sigma^2_{ij}}, \tag{46}$$

where $\Delta_{QCD} = y_{measured} - y_{MC}$. The weights w^j given for each distribution in Table 8 for JETSET and Table 11 for HERWIG are used to artificially increase the errors if there are systematic differences between the Monte Carlo prediction and the measurement. This is the method by which the

systematic discrepancies are propagated to the Monte Carlo parameter fit errors.

Since $\bar{\delta}$ is also measured for various values of κ, the correlations here are also taken into account so that

$$\chi^2_{\bar{\delta}} = \sum_{ij} \left(\widetilde{\Delta}_{\bar{\delta}}\right)_i \left(M^{-1}_{\bar{\delta}}\right)_{ij} \left(\Delta_{\bar{\delta}}\right)_j , \quad (47)$$

with the indices i and j running over the values of κ and $\Delta_{\bar{\delta}} = \bar{\delta}_{\text{measured}} - \bar{\delta}_{\text{predicted}}$. The inverse error matrix $M^{-1}_{\bar{\delta}}$ is built from the statistical correlation coefficients of $\bar{\delta}$ among κ values given in Table 20 and the errors quoted in Table 1. The value of $\delta_{\text{predicted}}$ is calculated from

$$\left(\bar{\delta}_{\text{predicted}}\right)^2 = \sum_{\text{f=uds}} \frac{\Gamma_{\text{f}}}{\Gamma_{\text{had}}} \left[\delta_{\text{f}} (1 + k_{\text{f}})\right]^2 + \frac{\Gamma_{\text{c}}}{\Gamma_{\text{had}}} \delta_{\text{c}}^2 + \frac{\Gamma_{\text{b}}}{\Gamma_{\text{had}}} \delta_{\text{b}}^2 \quad (48)$$

The prediction of $\bar{\delta}$ is based on the measurements of δ_{b} and δ_{c} as well as the hadronisation model predictions of the light flavours. The heavy flavour charge separations are allowed to vary within their errors through the term χ^2_{heavy} in (44).

As mentioned in Sect. 3.3, the b and c quark charge separations are correlated among each other and there are correlations between various values of κ. Thus

$$\chi^2_{\text{heavy}} = \sum_{\text{fgij}} \left(\widetilde{\Delta}_{\text{heavy}}\right)^i_{\text{f}} \left(M^{-1}_{\text{heavy}}\right)^{\text{fg}}_{ij} \left(\Delta_{\text{heavy}}\right)^j_{\text{g}} , \quad (49)$$

where the indices f and g run over the two heavy quark flavours and i and j run over the values of κ. The inverse error matrix M^{-1}_{heavy} is built from the correlation matrix in Table 21 and the errors from Table 5; $\Delta_{\text{heavy}} = (\delta_{\text{f}})_{\text{measured}} - (\delta_{\text{f}})_{\text{fit}}$ where the flavour f is one of the two heavy flavours. In this case, the charge separation is not predicted but allowed to move within their measurement errors in the fit and as constrained by δ which is computed using $(\delta_{\text{f}})_{\text{fit}}$.

The minimization of χ^2_{sep} gives the values of the charge separations for various κ values. Those for κ = 1.0 are shown in Table 19.

B.2 Fit of $\sin^2\theta^{\text{eff}}_{\text{w}}$

In order to obtain $\sin^2\theta^{\text{eff}}_{\text{w}}$ from $\langle Q_{\text{FB}}\rangle$, predictions for $A^{\text{f}}_{\text{FB}}\Gamma_{\text{f}}/\Gamma_{\text{had}}$ as a function of $\sin^2\theta^{\text{eff}}_{\text{w}}$ are first obtained from ZFITTER. Together with the charge separations this allows a prediction of $\langle Q_{\text{FB}}\rangle$ as given in (3). The final fit of $\sin^2\theta^{\text{eff}}_{\text{w}}$ is obtained by repeating the full fit adding an additional term to (44)

$$\chi^2_{\langle Q_{\text{FB}}\rangle} = \sum_{\text{e}} \sum_{ij} \left(\widetilde{\Delta}_{\langle Q_{\text{FB}}\rangle}\right)_{ie} \left(M^{-1}_{\langle Q_{\text{FB}}\rangle}\right)_{ije} \left(\Delta_{\langle Q_{\text{FB}}\rangle}\right)_{je} , \quad (50)$$

where $\Delta_{\langle Q_{\text{FB}}\rangle} = \langle Q_{\text{FB}}\rangle_{\text{measured}} - \langle Q_{\text{FB}}\rangle_{\text{predicted}}$. The sum runs over the three energies indicated by the index e and the various κ values indicated by the indices i and j. The statistical correlation coefficients of $\langle Q_{\text{FB}}\rangle$ among κ values are given in Table 22 and the error matrix $M^{-1}_{\langle Q_{\text{FB}}\rangle}$ is built from this and the errors from Tables 15 and 1.

B.3 Test of κ *dependence of* $\sin^2\theta^{\text{eff}}_{\text{w}}$

In order to determine if there is a κ dependence of $\sin^2\theta^{\text{eff}}_{\text{w}}$, the value of $\sin^2\theta^{\text{eff}}_{\text{w}}$ is computed for various values of κ from the final fitted values of the separations and the experimental measurements of $\langle Q_{\text{FB}}\rangle$. The relative errors between $\sin^2\theta^{\text{eff}}_{\text{w}}$ for κ = 1.0 and all other values of κ are computed as

$$\sigma^2_{\text{rel}} = \sigma^2_{\kappa=1} + \sigma^2_{\kappa} - 2\rho_{\langle Q_{\text{FB}}\rangle}\sigma_{\kappa=1}\sigma_{\kappa}, \quad (51)$$

where $\rho_{\langle Q_{\text{FB}}\rangle}$ is the correlation between measured values of $\langle Q_{\text{FB}}\rangle$ for various values of κ as given in Table 22. The resulting error is zero for κ = 1.0 and represented by the solid error bars for all other values of κ in Fig. 12.

References

1. R.D. Field and R.P. Feynman, Nucl. Phys. B136 (1978) 1.
2. J.P. Berge et al., Nucl. Phys. B184 (1981) 13;
   J.-P. Albanese et al., (EMC Coll.) Phys. Lett. B144 (184) 302.
3. ALEPH Collaboration, D. Decamp et al., Phys. Lett. B259 (1991) 377.
4. DELPHI Collaboration, P. Abreu et al., Phys. Lett. B277 (1992) 231.
5. OPAL Collaboration, P.D. Acton et al., Phys. Lett. B294 (1992) 436.
6. ALEPH Collaboration, D. Buskulic et al., Phys. Lett. B335(1994) 99.
7. OPAL Collaboration, R. Akers et al., Z. Phys. C67 (1995) 365.
8. DELPHI Collaboration, P. Abreu et al., Z. Phys. C65 (1995) 569.
9. ALEPH Collaboration, D. Decamp et al., Phys. Lett. B284 (1992) 177.
10. DELPHI Collaboration, P. Abreu et al., Phys. Lett. B322 (1994) 459.
11. ALEPH Collaboration, D. Buskulic et al., Phys. Lett. B356 (1995) 409;
    ALEPH Collaboration, D. Buskulic et al., CERN-PPE/96-030, submitted to Phy. Lett. B;
    ALEPH Collaboration, D. Buskulic et al., "B^0_d Mixing with Jet Charge and Lepton Correlations," submitted to HEP95, EPS 0409, 27 July– 2 August, 1995, Brussels, Belgium.
12. OPAL Collaboration, R. Akers et al., Phys. Lett. B327(1994) 411.
13. DELPHI Collaboration, P. Abreu et al., CERN-PPE/96-006, submitted to Z. Phys. C.
14. D. Bardin et al, CERN TH 6443-92, (1992).
15. The LEP Collaborations, Phys. Lett. B276 (1992) 267.
16. G.Batignani et al., Conf. Record of the 1991 IEEE Nuclear Science Symp., (November 1991, Santa Fe, NM, USA), IEEE Trans. on Nuclear Science v.NS 39(4-5), Aug. and Oct. 1992, Vol. 1, 438; ALEPH Collaboration, D. Buskulic et al., Phys. Lett. B313 (1993) 535.
17. T. Sjöstrand, Comp. Phys. Comm. 82 (1994) 74;
18. B.R. Webber, Nucl. Phys. B 234 (1984) 492;
    G. Marchesini et al., Comp. Phys. Comm. 67 (1992) 465.
19. ALEPH Collaboration, D. Decamp et al., Nucl. Inst. Meth. A286 (1990) 121.
20. ALEPH Collaboration, D. Buskulic et al., Nucl. Instr. Meth. A 360 (1995) 481.
21. ALEPH Collaboration, D. Buskulic et al., Z. Phys. C62 (1994) 179.
22. J. E. Campagne and R. Zitoun, Z. Phys. C43 (1989) 469.
23. ALEPH Collaboration, D. Buskulic et al., Z. Phys. C 55 (1992) 209. Data have been updated with events collected through 1992.
24. W.B. Atwood et al, Nucl. Inst. Meth. A306 (1991) 446.
25. ALEPH Collaboration, D. Decamp et al., Phys. Lett. B231 (1989) 519.
26. ALEPH Collaboration, D. Buskulic et al., Phys. Lett. B352 (1995) 479.
27. C. Peterson et al, Phys. Rev. D 27 (1983) 105.
28. K. Hikasa et al., Review of Particle Properties, Phys. Rev. D45 (1992).
29. M. Gell-Mann, Phys. Rev. **92** (1953) 833;
    K. Nishijima and T. Nakano, Prog. Th. Phys. **10** (1953) 581.
30. B. Andersson, et. al., Physica Scripta 32 (1985) 574.
31. ALEPH Collaboration, D. Buskulic et al., Z. Phys. C 64 (1994) 361.
32. ALEPH Collaboration, D. Buskulic et al., Z. Phys. C 66 (1995) 355.
33. DELPHI Collaboration, P. Abreu et al., Z. Phys. C 65 (1995) 587.
34. OPAL Collaboration, P. Acton et al., Z. Phys. C 56 (1992) 521.
35. ALEPH Collaboration, D. Buskulic et al., Phys. Lett. B292 (1992) 210.
36. A. Djouadi et. al, Z. Phys. C67 (1995) 123.